AD-A068 108 ANALYTICAL METHODS INC BELLEVUE WASH F/G 20/4
AN INVESTIGATION OF SEPARATION MODELS FOR THE PREDICTION OF CL --ETC(U)
APR 79 F A DVORAK, B MASKEW, B M RAO DAAG29-76-C-0019
UNCLASSIFIED ARO-13225.2-E NL

| OF |
ADA
068108

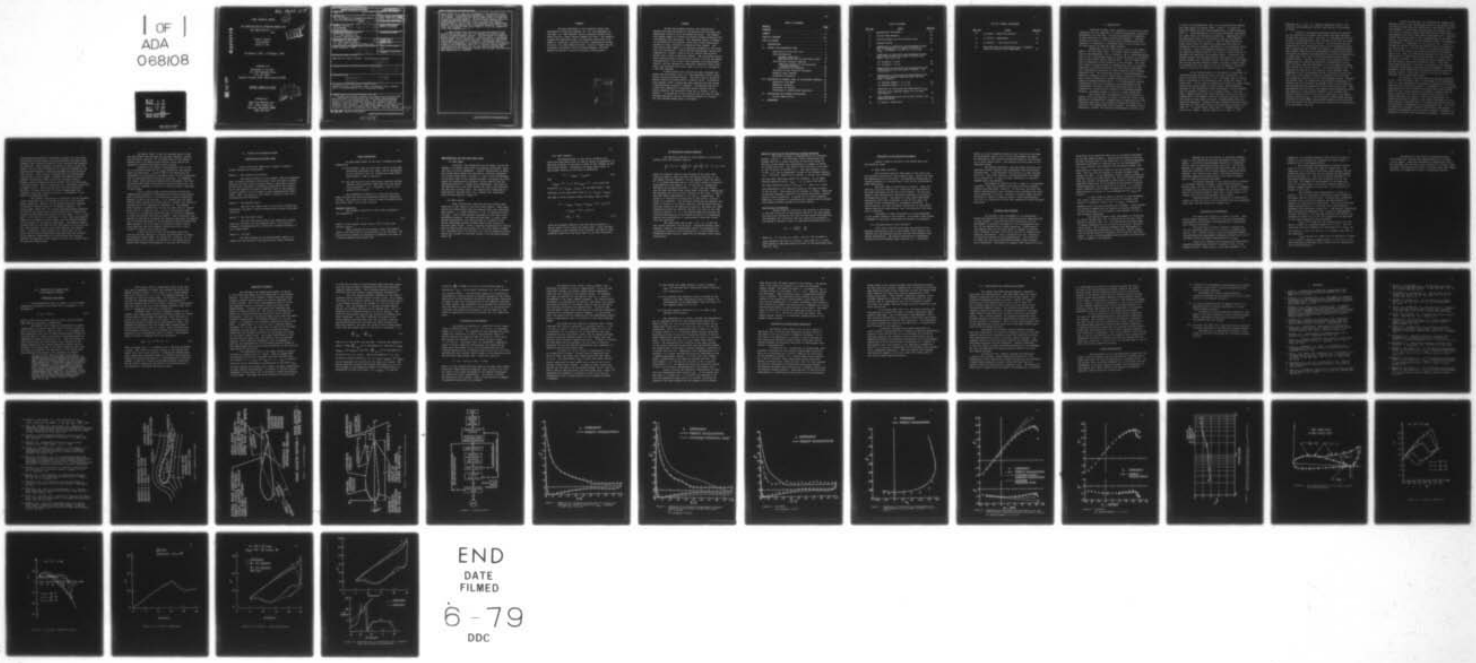

END
DATE
FILMED
6-79
DDC

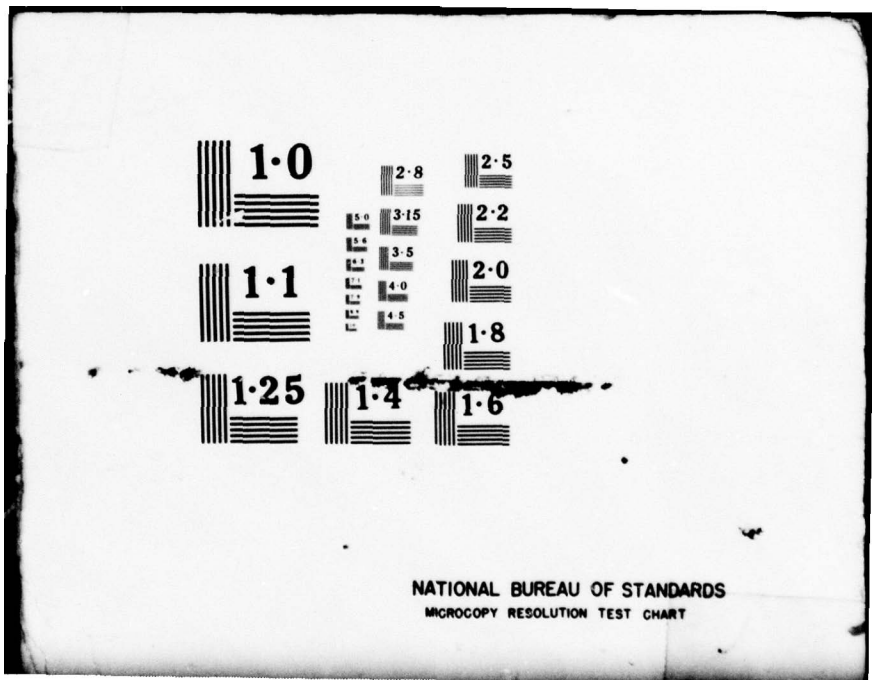
1·0
1·1
1·25
2·8
3·15
3·5
4·0
4·5
5·0
2·5
2·2
2·0
1·8
1·4
1·6
NATIONAL BUREAU OF STANDARDS
MICROCOPY RESOLUTION TEST CHART

ARO 13225.2-E

(12)

FINAL TECHNICAL REPORT

"AN INVESTIGATION OF SEPARATION MODELS FOR THE PREDICTION OF $C_{\ell_{MAX}}$"

LEVEL II

FRANK A. DVORAK
BRIAN MASKEW
BALUSU M. RAO

16 FEBRUARY, 1976 - 15 FEBRUARY, 1979

PREPARED FOR:

DEPARTMENT OF THE ARMY
U.S. ARMY RESEARCH OFFICE
P.O. BOX 12211
RESEARCH TRIANGLE PARK, NORTH CAROLINA 27709

CONTRACT DAAG29-76-C-0019

PREPARED BY:

ANALYTICAL METHODS, INC.
100 - 116TH AVENUE S.E.
BELLEVUE, WASHINGTON 98004
(206) 454-6119

SECURITY CLASSIFICATION OF THIS PAGE (When Data Entered)

REPORT DOCUMENTATION PAGE

READ INSTRUCTIONS BEFORE COMPLETING FORM

1. REPORT NUMBER (6)	2. GOVT ACCESSION NO. / 3. RECIPIENT'S CATALOG NUMBER (9)
4. TITLE (and Subtitle): "An Investigation of Separation Models for the Prediction of $C_{l_{max}}$" (CL sub max)	5. TYPE OF REPORT & PERIOD COVERED: FINAL TECHNICAL REPORT, 16 Feb. '76 — 15 Feb. '79 / 6. PERFORMING ORG. REPORT NUMBER
7. AUTHOR(s) (10): Frank A. Dvorak, Brian Maskew, Balusu M. Rao	8. CONTRACT OR GRANT NUMBER(s) (15): DAAG29-76-C-0019
9. PERFORMING ORGANIZATION NAME AND ADDRESS: Analytical Methods, Inc., 100 - 116th Avenue S.E., Bellevue, Washington 98004	10. PROGRAM ELEMENT, PROJECT, TASK AREA & WORK UNIT NUMBERS
11. CONTROLLING OFFICE NAME AND ADDRESS (11): Department of the Army, U.S. Army Research Office, P.O. Box 12211, Research Triangle Park	12. REPORT DATE: April, 1979 / 13. NUMBER OF PAGES: 50
14. MONITORING AGENCY NAME & ADDRESS (if different from Controlling Office): North Carolina 27709 (12) 58p.	15. SECURITY CLASS. (of this report): None / 15a. DECLASSIFICATION/DOWNGRADING SCHEDULE

16. DISTRIBUTION STATEMENT (of this Report)

Approved for public release; distribution unlimited.

(18) ARO

17. DISTRIBUTION STATEMENT (of the abstract entered in Block 20, if different from Report)

(19) 13225.2-E

18. SUPPLEMENTARY NOTES

THE VIEW, OPINIONS, AND/OR FINDINGS CONTAINED IN THIS REPORT ARE THOSE OF THE AUTHOR(S) AND SHOULD NOT BE CONSTRUED AS AN OFFICIAL DEPARTMENT OF THE ARMY POSITION, POLICY, OR DECISION, UNLESS SO DESIGNATED BY OTHER DOCUMENTATION.

19. KEY WORDS (Continue on reverse side if necessary and identify by block number)

Separated flows; aerodynamic loads; aerodynamic stall; dynamic stall; viscous/potential flow interaction scheme

20. ABSTRACT (Continue on reverse side if necessary and identify by block number)

Steady and unsteady analyses and computational methods have been developed for calculating the flow about two-dimensional airfoils up to and beyond the stall. The steady-flow method adopts an iterative procedure between the potential flow and boundary layer solutions. The separated region is modeled in the potential flow analysis using free vortex sheets which require an inner iteration to establish their shapes. The free vortex → next Page 1/B

DD FORM 1 JAN 73 1473 EDITION OF 1 NOV 65 IS OBSOLETE

SECURITY CLASSIFICATION OF THIS PAGE (When Data Entered)

392078

sheet length is an important parameter in the potential flow calculation. Calculated and experimental results are compared for a GA(W)-1 airfoil and for several NACA airfoil series over a range of Reynolds numbers. The calculated results, which include pressure distributions as well as force and moment characteristics, are in very close agreement with experimental results, and are obtained for reasonable computing costs; typically, one incidence data point takes 15 to 20 c.p. seconds on a CDC 7600 computer.

A quasi-steady flow analysis has been developed for predicting the dynamic stall of a two-dimensional airfoil undergoing a pitching harmonic motion. The flow field is solved at several angles of attack during a complete cycle. A potential flow program, using a separation wake obtained from the steady viscous/potential program is adopted. Preliminary results on a NACA 0012 undergoing a sinusoidal motion indicate the expected trends of the hysteresis loops for C_ℓ versus α and C_m versus α. A discussion on the criterion for the onset of leading-edge separation and the differences between the leading- and trailing-edge separations is included.

FOREWARD

The work described in this technical report was performed by Analytical Methods, Inc. for the Department of the Army, U.S. Army Research Office, Research Triangle Park, North Carolina, under Contract DAAG29-76-C-0019. The research program was undertaken under the technical cognizance of Dr. Robert E. Singleton, Associate Director, Engineering Sciences Division, U.S. Army Research Office. Frank A. Dvorak was the Principal Investigator and the Program Manager, and Brian Maskew and Balusu M. Rao were Associate Investigators.

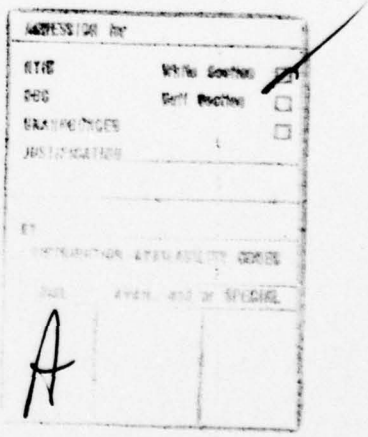

SUMMARY

Steady and unsteady analyses and computational methods have been developed for calculating the flow about two-dimensional airfoils up to and beyond the stall. The steady-flow method adopts an iterative procedure between potential flow and boundary layer solutions. The separated region is modeled in the potential flow analysis using free vortex sheets which require an inner iteration to establish their shapes. The free vortex sheet length is an important parameter in the potential flow calculation. Calculated and experimental results are compared for a GA(W)-1 airfoil and for several NACA airfoil series over a range of Reynolds numbers. The calculated results, which include pressure distributions as well as force and moment characteristics, are in very close agreement with experimental results, and are obtained for reasonable computing costs; typically, one incidence data point takes 15 to 20 c.p. seconds on a CDC 7600 computer.

A quasi-steady flow analysis has been developed for predicting the dynamic stall of a two-dimensonal airfoil undergoing a pitching harmonic motion. The flow field is solved at several angles-of-attack during a complete cycle. A potential flow program, using a separation wake obtained from the steady viscous/potential program is adopted. Preliminary results on a NACA 0012 undergoing a sinusoidal motion indicate the expected trends of the hysteresis loops for C_ℓ versus α and C_m versus α. A discussion on the criterion for the onset of leading-edge separation and the differences between the leading- and trailing-edge separations is included.

TABLE OF CONTENTS

Section		Page
FOREWARD		i
SUMMARY		ii
TABLE OF CONTENTS		iii
LIST OF FIGURES		iv
I	INTRODUCTION	1
II	STEADY FLOW SEPARATION MODEL	7
	Description of the Real Flow	7
	Basic Assumptions	8
	Boundary Conditions	8
	Approximations for the Free Shear Layer	9
	The Governing Integral Equation	11
	Numerical Solution of the Governing Integral Equation	12
	Calculation of Pressures	12
	Structure of the Iterative Procedure	13
	Boundary Layer Methods	14
	Discussion of Results	16
III	PREDICTION OF DYNAMIC STALL ON OSCILLATING AIRFOILS	19
	Separation Flow Model	19
	Numerical Procedure	21
	Discussion of Results	23
	Discussion on Leading-Edge Separation	26
IV	CONCLUSIONS AND FURTHER APPLICATIONS	28
	Further Applications	29
V	REFERENCES	31

LIST OF FIGURES

Fig. No.	Title	Page No.
1	Mathematical Flow Model	34
2	Initial Wake Geometry	35
3	Vorticity Model for the Potential Flow	36
4	Program Outline	37
5	Comparison of Calculated and Experimental Pressure Distributions on a GA(W)-1 Airfoil at $C_{\ell_{max}}$. Incidence = 19.06^0; Re = 6.3×10^6 . .	38
6	Comparison of Calculated and Experimental Pressure Distributions on a GA(W)-1 Airfoil Post Stall: Re = 6.3×10^6	
	(a) Incidence = 20.05^0	39
	(b) Incidence = 21.14^0	40
7	Comparisons of Calculated and Experimental Drag Characteristics for the GA(W)-1 Airfoil: Re = 6.3×10^6	41
8	Comparisons of Calculated and Experimental Lift and Pitching Moment Characteristics for the GA(W)-1 Airfoil.	
	(a) Reynolds Number = 6.3×10^6	42
	(b) Reynolds Number = 2.1×10^6	43
9	Comparison of Calculated and Experimental $C_{\ell_{max}}$ Variation with Reynolds Number for the NACA 4412 Airfoil	44
10	Panel Representation of the Airfoil Surface and Separated Region	45
11	C_ℓ Versus α (NACA 0012)	46

LIST OF FIGURES (CONCLUDED)

Fig. No.	Title	Page No.
12	C_m Versus α (NACA 0012 Airfoil)	47
13	C_ℓ Versus α (Experiment)	48
14	C_ℓ Versus α - Oscillatury Motion	49
15	The Phase Lag (ϕ) Distribution over a Complete Cycle to Correlate with Experiment	50

I. INTRODUCTION

Turbulent boundary layer separation is one of the least understood but most important of fluid flow phenomena related to aerodynamic lift and drag. Its accurate modeling is essential to the estimation of airborne vehicle performance. Currently, reliance is placed on wind tunnel tests to determine the consequences of separation, a procedure which is not entirely free of doubt because of Reynolds number effects.

Separations can be classified as being of two types--bubble, and free shear layer. The bubble type of separation is seen in two-dimensional flow on airfoils, and in three-dimensional flow in the trailing-edge region of wings and rotors at incidence, and on bluff bodies having rapid closure. The free shear layer type of separation occurs primarily in two regions. The first such region is where geometric considerations such as wing-body junctions or hub-pylon-fuselage junctions cause considerable flow interference resulting in vortex formation and a strongly separated flow. The second case arises on three-dimensional bodies at incidence, such as delta wings of bodies of revolution where rapid convergence of surface streamlines results in a greatly thickened boundary layer. It is postulated by several investigators that with convergence and coalescence of the streamlines, the strong cross-flow velocities result in the formation of a vortex which, because of the adverse pressure gradient, increases rapidly in size as it moves downstream.

This latter type of separation is very difficult to predict (with the exception of cases in which the vortex layer separation is preceded by a bubble-type of separation as in the wing-body junctions), and successful theoretical modeling is limited to the leading-edge vortex problem. The bubble type of separation, however, has received considerable attention, and,

at least in two-dimensional flow, can be predicted and modeled with some degree of success (Refs. 1 and 2). A simple yet effective method has even been demonstrated in three dimensions (Ref. 3). These methods all use criteria developed from boundary layer theory for separation prediction. Representation of the separation region in the potential flow by each method differs basically only in detail. Each of these methods employs source fluid to simulate the separated flow with the assumption that the pressure everywhere in the separated region is constant. None of the methods calculates the pressure in the separation region directly, but relies on some criterion to determine the separated flow pressure devel. In general, the methods predict the upstream pressure distribution in a satisfactory manner once a suitable source "out-flow" has been chosen. None of the existing methods, however, provides a direct analysis procedure for the prediction of the aerodynamic characteristics of airfoils for angles of attack at or beyond $C_{\ell_{max}}$.

As the forward speed of a helicopter is increased, the retreating blade encounters lower and lower velocities. In order to produce its portion of lift, the blade angle of attack must be increased on the retreating side, which will result in blade stall. If the angle of attack of an airfoil or other lifting surface oscillates around the stall angle, large hysteresis develops in the aerodynamic forces and moments, and this phenomenon is generally referred to as "dynamic stall". Over the years, numerous wind tunnel tests provided a wealth of data and information on the dynamic stall of oscillating airfoils for a wide range of mean angles of attack, unsteady amplitudes, and reduced frequencies. Perhaps the most extensive and significant test data on a NACA 0012 airfoil were provided by Halfman et al. (Ref. 4). In recent years, Carta (Ref. 5), Windsor (Ref. 6), Liiva et al. (Refs. 7 and 8), Martin et al. (Ref. 9), and

McCroskey et al. (Ref. 10), reported additional data on conventional two-dimensional airfoils oscillating at high angles of attack.

Several investigators developed theoretical analyses for the prediction of dynamic stall based upon some empirical factors from the test data. Ham (Ref. 11) developed an analysis in which he represented the stall process by the vorticity shed from the leading edge of the airfoil. The initiation and the termination of the leading-edge vorticity was determined empirically, neglecting the viscous flow effects. Satisfactory agreement between theoretical and experimental pressure distribution and forces and moments was demonstrated for airfoils experiencing a sudden onset flow, and for airfoils performing oscillatory pitching motion. However, the success of the analysis was dependent upon the appropriate empirical representation of the shed vorticity, and the development of any non-empirical theory must include the viscous effects. Liiva and Davenport (Ref. 12) developed an analysis of lift behavior during dynamic stall, depending only on instantaneous values of angles of attack and pitch rate, and showed satisfactory agreement with test data for sinusoidal oscillation over a wide frequency range. Erickson and Reading (Ref. 13) showed that the dominant charactistic of leading- and trailing-edge type dynamic stall was the effect of the accelerated flow generated by the non-zero pitch rate. They hypothesized that the pitch rate induced flow acceleration delays the adversity of the pressure gradient on the leeward side, thereby causing a delay of the stall, resulting in the experimentally observed $C_{\ell_{max}}$. They developed a quasi-steady analysis in which the time history effects were lumped into one discrete past time event, and the acceleration flow effect was represented by an equivalent time lag.

Johnson and Ham (Ref. 14) discussed the evidence and dominant effect of the leading-edge vortex on the dynamic stall. The dynamic stall delay was attributed to the delay in the forward movement of the bubble trailing edge due to pitch rate ($\dot{\alpha}$), while the bubble leading edge moves to the airfoil more at approximately the static stall angle regardless of $\dot{\alpha}$. They postulated that the process of flow reenergization in turbulent mixing in the bubble aft of the transition point, and subsequent reattachment, is independent of the external flow. They developed an analysis relating the dynamic stall to the delay of the transition; i.e., to the effect of the pressure gradient due to $\dot{\alpha}$ on the location of transition points in the bubble. Carta et al. (Ref. 15) reduced the measured lift and pitching moment data on a NACA 0012 oscillating model to a function of the angle of attack, α, the angular velocity parameter, $b\dot{\alpha}/v$, and the angular acceleration parameter, $b\ddot{\alpha}/v^2$. They used this generalized form of the data to reconstruct the measured sinusoidal aerodynamic response with good agreement. Similar procedures could probably be developed for other airfoils and motions; however, each class of airfoil and motion require a different set of experimental data.

In contrast to the semi-empirical analyses discussed so far, Crimi and Reeves (Ref. 16) and Shamroth and Kreskovsky (Ref. 17) have developed more funamental analyses using viscous/potential flow interaction models. In Reference 16, a linearized representation of the potential flow model and a quasi-steady model for the viscous regions were adopted, assuming that the rate of growth of the dead-air region at the onset of the leading-edge stall was equal to the free-stream speed. Although the procedure produces a qualitative agreement with the basic features of dynamic stall, its theoretical predictions are in quantitative disagreement with experimental data. This lack of correlation, perhaps, could be attributed to the several simplifying assumptions that they have included in boundary and potential flow models and calculation procedures. Shamroth and

and Kreskovsky developed a technique to predict the flow about oscillating airfoils using an inviscid/viscous flow model which assumes a weak viscous correction to the inviscid flow pressure distribution. Their approach is similar to that of Crimi and Reeves, but they have incorporated an improved treatment of the separated flow regions, transition phenomena and the potential flow regions. Their results indicated that the leading-edge viscous flow is quasi-steady, although the imposed inviscid pressure distribution shows significant unsteady effects. However, their procedure failed to predict the flow field about a stalled airfoil, which is essential for a successful prediction of dynamic stall. They concluded that the weak-interaction solution, in which the effect of viscous displacement was ignored on the outer inviscid solution, is inadequate to represent the separated flows.

The inherent limitations of potential flow and boundary layer calculations can be overcome by the use of full Navier-Stokes equations. However, at the present time this technique is limited to laminar flows at low Reynolds numbers. In a recent paper, Mehta (Ref. 18) solved the Navier-Stokes equations in terms of the vorticity and stream function for laminar flow around a modified NACA 0012 airfoil for two cases: (1) $R = 5{,}000$ and $k = 0.5$; and (2) $R = 10{,}000$ and $k = 0.25$, where the Reynolds number (R) is based on airfoil chord, and the reduced frequency of oscillation (k) is based on half-chord. The reported computational time on a CDC 7600 for one time step for the second case was 1.086 minutes, with 885 time steps used for one complete cycle. Definitely, there seems to be a great deal one can learn from the full Navier-Stokes solutions from the standpoint of the physical understanding of the detailed flow process; however, the approach is too expensive to use on a routine basis for practical applications.

McCroskey (Refs. 19 and 20) reviewed many of these new developments and the empirical methods currently used by the helicopter industry. He concluded that all the present methods have to be applied with caution, since they do not adequately represent the dynamic stall process.

Because of the current unsatisfactory state of the art in separation modeling for $C_{\ell_{max}}$ prediction, the present study was undertaken. It has as one of its objectives the development of a separation flow model which can be incorporated into a viscous/potential interaction analysis. To implement this study, three separation models were considered. The first two models were based on distributed source singularities, but were quickly dismissed in favor of a vorticity model, described in this report.

Also, a quasi-steady viscous/potential interactive computational procedure is developed for predicting the dynamic stall characteristics of a two-dimensional airfoil undergoing harmonic pitching oscillations. It is assumed that the upper surface moves towards the leading edge at a slower rate during an unsteady motion as suggested in Reference 14. The dynamic stall process is predicted by solving the flow field at several points during a complete cycle. At each instantaneous angle of attack, a corresponding modified angle of attack is computed to take into account the time lag effect. Then a potential flow program is used which satisfies the boundary conditions corresponding to the modified angle of attack obtained from the steady flow CLMAX program. The flow model is designed to handle typical large amplitude and low frequency values which are of great interest in dynamic stall predictions.

A major portion of the work performed under this contract has been reported in several Interim Technical Reports and technical papers (Refs. 21 through 25). However, for the completeness of the report, the details of the steady and unsteady flow analyses are presented in the next two sections.

II. STEADY FLOW SEPARATION MODEL

Description of the Real Flow

A flow field with separation is shown in Figure 1. Several regions are identifiable.

Region 1: The Potential Flow Region

The region exterior to the boundary layer and separated wake is almost precisely irrotational, since the shear is everywhere so low that viscous stresses impart a negligible rotation to the fluid (originally irrotational upstream of the airfoil). All of the regions are almost solenoidal since we are assuming the Mach number to be low enough to make compressibility negligible. Thus, the region is very nearly a potential flow (i.e., irrotational and solenoidal).

Region 2: The Boundary Layer

The thin flow region next to the airfoil surface has high shear, and hence, viscous stresses which create significant vorticity.

Region 3: The Free Shear Layer

The thin flow region fed by the separating boundary layer has rotation, but only moderate shear. The vorticity transport is predominantly by convection, although diffusion is not insignificant.

Region 4: The Wake

The wake between the two shed boundary layers is a region with low vorticity and insignificant viscous stresses.

Basic Assumptions

An approximate model of the flow is defined by these assumptions:

(i) The boundary layer and free shear layers do not have significant thickness and, hence, can be represented as slip surfaces; that is, streamlines across which there exists a jump in velocity.

(ii) The wake does not have significant vorticity and has constant total pressure (lower than the free stream total pressures). It is, therefore, taken to be a potential flow region.

The mathematical problem is to find the vorticity sheet strength such that the appropriate boundary conditions are met. The position of the vorticity sheet representing the free shear layer is not known a priori.

Boundary Conditions

The boundary condition for the airfoil surface is flow tangency or

$$\vec{V} \cdot \vec{n} = 0 \qquad (2.1)$$

where $\vec{n}$ = unit surface normal vector, and $\vec{V}$ is the total velocity vector.

When allowing for the boundary layer displacement effect, the right side of this equation will be non-zero. The free vorticity sheets are located on streamlines and there is no static pressure drop across them.

Approximations for the Free Shear Layer

(i) Wake Shape

Initially, the streamlines are not known, and so the shapes of the shear layers must be obtained iteratively, starting from an initial assumption. Earlier calculations in which the vortex sheet shapes were obtained by iteration suggested the initial shape shown in Figure 2. This is now incorporated as the basic wake in the computer program. The upper and lower sheets are represented by parabolic curves passing from the separation points to a common point downstream. The slope at the upstream end is the mean between the free stream direction and the local surface slope. The common point downstream is positioned on the mean wake line, distance, WL, downstream from the wake midpoint (Figure 2).

(ii) Wake Length

Early calculations indicated that the results were sensitive to the length of the free vortex sheets. Good correlation with experimental data was obtained only with relatively short wakes, i.e., wakes extending .1c to .2c beyond the trailing edge. Such a model appears reasonable in the light of experimental evidence: the separated wake does, in fact, close quickly downstream of the trailing edge as a result of the strong entrainment process brought about by the rotation in the free shear layers. After a thorough investigation of several ways of defining the wake length, WL, the final model is based on a "fineness ratio" of the wake; i.e., WL is obtained by multiplying the "height" of the wake (Figure 2) by the wake fineness ratio, WF.

(iii) Wake Pressure

The approximation of zero static pressure drop across the free shear layer is used to obtain an expression for the total pressure in the wake in terms of the strength of the free vortex sheets. Considering the upper shear layer, if the average velocity in the layer is denoted by

$$\bar{V} = (V_{outer} + V_{inner})/2 \tag{2.2}$$

then

$V_{outer} = \bar{V} + \gamma_u/2$, and $V_{inner} = \bar{V} - \gamma_u/2$, since the vorticity, $\gamma_U = V_{outer} - V_{inner}$, on the upper sheet. (The vorticity in the lower shear layer is $\gamma_L = V_{inner} - V_{outer}$.) The jump in total pressure across the shear layer is then

$$\begin{aligned} \Delta H &= H_{inner} - H_{outer} = p_{inner} + \rho(\bar{V} - \gamma_u/2)^2/2 \\ &\quad - \{p_{outer} + \rho(\bar{V} + \gamma_u/2)^2/2\} \\ &= -\rho\bar{V}\gamma_U = \rho\bar{V}\gamma_L \end{aligned} \tag{2.3}$$

given the boundary condition that the static pressure, p, has no jump in value across the shear layer. Since the wake is assumed to have constant total pressure, the jump in total pressure across the free shear layer is the same everywhere.

The Governing Integral Equation

The boundary condition of flow tangency on the airfoil surface gives the integral equation

$$\int_C K\,\gamma(s)\,ds + \gamma_L\left(\int_L K\,ds - \int_U K\,ds\right) + \vec{V}_\infty \cdot \vec{n} = V_n \quad (2.4)$$

where the constant value of the strength of the lower free vorticity sheet is used and where the kernel function, K, is the normal velocity component (at the boundary point for which $\vec{V} \cdot \vec{n}$ is being enforced) due to a unit point vortex at the point associated with the element, δs, of the line of integration, and where the integration paths, C, L and U are the airfoil and the lower and upper free vortex sheet locations, respectively. The unknowns are the vorticity strengths on the curve, C, and on the free sheets represented by $\gamma(s)$ and γ_L, respectively. The former is a function of the position of the airfoil, and the latter is a constant. Two auxiliary conditions are applied; the first is related to the Kutta condition, and specifies that the vorticity values at the separation points on the upper and lower surfaces are equal but opposite and have the value at the free vorticity sheets; i.e., γ_L. The second condition concerns the vorticity distribution on the airfoil surface in the separated region; this distribution is constrained to start and finish with zero vorticity.

The right-hand side of Eqn. (2.4), V_n, is zero for the initial potential flow solution. Following boundary layer analysis, however, the displacement effect is represented by a piecewise constant source distribution; V_n then becomes the integrated normal velocity induced by the boundary layer source distribution.

Numerical Solution of the Governing Integral Equation

The airfoil contour is represented by an inscribed polygon, Figure 3. The individual panels representing the polygon each has a linear variation of vorticity across it. The free vortex sheets are represented by a number of panels of uniform vorticity. The value of the vorticity at the start of the i^{th} panel is denoted by γ_i. Thus the function, $\gamma(s)$, in Eqn. (2.4) can be expressed in terms of the unknown sequence, $\{\gamma_i\}$. Initially, there are N+1 unknown γ_i values (for N panels), but auxiliary conditions remove two unknowns: at the upper surface separation point, $\gamma_{sep} = -\gamma_L$ (γ_L being the value at the lower separation point), and $\gamma_{N+1} = 0$. Also, the γ value just downstream of the separation point on the upper surface is set to zero. Thus there are N-1 unknown γ_i values. Enforcing the surface boundary condition at the panel mid-points (control points) gives N equations. A square set of linear algebraic equations is obtained by introducing one unknown source strength distributed uniformly around the airfoil surface.

Calculation of Pressures

Having found the vorticity, the velocity at any point in the flow field can be evaluated by adding to the free stream the velocities induced by the vorticity and source distributions. The pressures are calculated from the velocities according to the Bernoulli equation, which is expressed non-dimensionally as

$$C_p = 1 - \left(\frac{V}{V_\infty}\right)^2 + \frac{\Delta H}{q_\infty}$$

where $C_p = (p - p_\infty)/q_\infty$, $q_\infty = \frac{1}{2}\rho V_\infty^2$, and ΔH = the increase in total pressure over that at infinity. Note that $\Delta H = 0$ everywhere except in the wake region for which it was previously shown that $\Delta H = \rho \bar{V} \gamma_L$.

Structure of the Iterative Procedure

Figure 4 shows an outline of the method which has two iterative loops.

(i) Wake Shape Iteration

The iteration loop for wake shape is the inner loop and involves the potential flow analysis only. Within this loop the separation points are fixed. The separation points may be located anywhere on a surface panel; they are not restricted to panel edge points.

The wake shape is calculated as follows. Using the previous vorticity distribution, velocities are calculated at the panel mid-points on the free vortex sheets. The new wake shape is then determined by piecewise integration, starting at the separation points. The upper and lower sheet downstream end points, which were coincident in the initial wake, are allowed to move independently in subsequent iterations. At each iteration, the wake influence coefficients at the surface control points are recalculated, and a new potential flow solution is obtained.

The number of wake iterations is an input parameter in the current version of the program. For several cases tested, a maximum of three wake iterations was proved to be adequate.

(ii) Viscous/Potential Flow Iteration

This outer iteration loop takes the potential flow pressure distribution over to the boundary layer analysis and returns with the separation points and with the boundary layer source distribution. The source distribution is determined directly from the boundary layer solution as $\sigma = d/ds(u_e\delta^*)$,

where u_e is the streamwise potential flow velocity at the edge of the boundary layer, and δ^* is the displacement thickness. The addition of this source distribution modifies the velocity, V_n, at each control point. The sources are set to zero in the separated region.

The program generates a new wake shape using the new separation points together with information from the previous iterated wake. A new potential flow solution is then obtained and so on. The outer iteration is terminated when the change in C_ℓ is below 1%. A limit of eight iterations is currently imposed within the program.

The program is usually run for a range of (increasing) incidence. Each new incidence case starts with the previous solution and wake model, Figure 4. In this way, the force and moment characteristics with incidence up to and beyond the stall, can be generated in one run. Multiple incidence cases are more efficient in terms of computing effort, taking approximately 15 to 20 c.p. seconds on the CDC 7600 computer for each converged data point.

Boundary Layer Methods

The boundary layer development on an arbitrarily-shaped two-dimensional lifting configuration with separated flow is very complex. A thorough and exact calculation of this development is properly the domain of the time-dependent solution to the general Navier Stokes equations. Unfortunately, the computer does not yet exist which is capable of handling such a problem, and even if one did, the cost in computer time would be astronomical. Such a calculation is not, therefore, of practical interest to the aerodynamicist. Less difficult or costly are the finite-difference boundary layer programs now in existence. The amount of computer time required for each

calculation still prohibits their use in an analysis procedure of the type reported herein. Having made the above evaluation, one must conclude that if the objective is a viscosity-dependent calculation procedure of practical use to the aerodynamicist for $C_{\ell_{max}}$ analysis, and, possibly for preliminary design, the method must be relatively simple to use and economic of computer time. This can only be achieved if integral boundary layer methods are used. In two-dimensonal flows, integral methods are typically about 100 times faster than finite-difference methods. They can, however, be expected to break down in the region of separation where none of the boundary layer methods (including three-dimensional) can be expected to be valid. It is anticipated, therefore, that integral methods will suffice for most applications of interest to the aerodynamicist for $C_{\ell_{max}}$ prediction.

In those cases of special interest to the aerodynamicist, such as the effect of area suction on boundary layer control or roughness (rivets, etc.) on $C_{\ell_{max}}$, alternative boundary layer calculation modules are available. These methods are called as needed into the overall calculation procedure. A brief description of the boundary layer methods is given in the following paragraphs.

The laminar boundary layer development is calculated by Curle's method (Ref. 26), an adaptation of the well known method of Thwaites (Ref. 27). The calculation proceeds either to laminar separation or to the end of the airfoil, whichever occurs first. The calculated boundary layer development is then interrogated to determine if transition, laminar separation or forced transition (boundary layer tripping) has taken place. If any of these phenomena have occurred, the downstream flow is assumed to be turbulent.

Methods for the calculation of turbulent boundary layers in two dimensions have been developed by many investigators. A review of these methods was made at a conference held in 1968 at Stanford University (Ref. 28). One of the methods, an integral method by Nash and Hicks (Ref. 29) compared very favorably with the more complex finite-difference methods. Now, several years later, the method remains an excellent approach for application to the current problem, both in terms of accuracy and speed.

If surface roughness or area suction are of interest, an alternate turbulent boundary layer method developed by Dvorak (Refs. 30 and 31) can be called. This method is capable of predicting the downstream development and the skin friction drag of a turbulent boundary layer over a rough surface, or a surface with area suction boundary layer control.

Turbulent boundary layer separation is predicted by either the Nash and Hicks or Dvorak methods when the calculated local skin friction coefficient reaches zero.

Discussion of the Results

The method was applied to a GA(W)-1 airfoil. This section shape represents a difficult test case and pressure distributions are available from experiments at NASA-Langley for a range of incidence.

The first set of results, Figures 5 through 8(a) are for a Reynolds number of 6.3×10^6 with a boundary layer trip at .08c. Figure 5 shows a very good agreement between the calculated and experimental pressure distribution at 19.06^0 incidence (which corresponds approximately to $C_{\ell_{max}}$).

Figure 6(a) compares the calculated and experimental pressure distributions at 20.05^0 incidence, which is just beyond the stall. Again there is very good agreement. For

comparison, the attached potential flow solution at this incidence is also plotted and indicates the large change in pressures due to the separated flow.

The calculated and experimental pressure distributions at 21.14^0 incidence are shown in Figure 6(b). The comparison is not as good as the other cases because the predicted separation point has not yet reached the experimental position at about .1c. The rate of forward movement of the calculated separation point with iteration at 21.14^0 was very slow. The sudden forward movement of the separation point in the experiment is just over a degree change in incidence (compare Figures 6(a) and 6(b)) and is difficult to predict in this case.

The calculated drag characteristic is given in Figure 7. This is obtained by integrating surface pressures and adding the skin friction drag. Pressure drag integration is known to be a difficult problem, and inaccuracies are apparent in comparison with experiment. The lift and pitching moment characteristics, on the other hand, show excellent agreement with experiment, Figure 8(a). The present calculations show considerable improvement over a previous Lockheed/NASA-Langley calculation. The attached potential flow solution is included in Figure 8(a) to put into perspective the magnitude of the change achieved by the new method.

Figure 8(b) shows the lift characteristics for the GA(W)-1 airfoil at a Reynolds number of 2.1×10^6. The calculations give good agreement with experiment up to $C_{\ell_{max}}$, but the turnover in the curve occurs 2 to 3 degrees later than in the experiment.

$C_{\ell_{max}}$ results for a NACA 4412 are presented in Figure 9 for a range of Reynolds numbers from 0.2×10^6 to 6.3×10^6. The calculated values agree very closely with the experimental curve from Reference 32.

The details of the history of separation point, lift coefficient, and the wake shape history are not shown in this report. These were presented in Reference 24 and it was concluded that for most cases of practical interest, about six outer (viscous/potential flow) and three inner (wake shape) iterations are adequate to obtain a convergent solution.

III. PREDICTION OF DYNAMIC STALL ON OSCILLATING AIRFOILS

Separation Flow Model

The instantaneous angle of attack, α, of an airfoil undergoing a sinusoidal oscillation with a frequency, ω, is expressed as

$$\alpha = \alpha_m + \bar{\alpha} \sin \omega t \tag{3.1}$$

where α_m and $\bar{\alpha}$ are the mean angle of attack and the angular amplitude of oscillation, respectively.

The dynamic stall process is predicted on a quasi-steady basis, by solving the flow field at several values of angle of attack during a complete cycle. It is assumed that the separation point over the upper surface moves towards the trailing edge at a slower rate during an unsteady motion as suggested by Johnson and Ham (Ref. 14). They attributed the stall angle delay and other dynamic stall features to the dynamic behavior of the laminar separation bubble which is formed at the leading edge on the upper surface as the angle of attack is increased, the same way as in the static case. They postulated the dynamic stall phenomena as follows:

> "As the rate of change of angle of attack is increased, there is a negligible delay before the laminar separation point reaches the airfoil leading edge, while the forward movement of the turbulent reattachment point is retarded, suggesting that the bubble elongates. Finally, the bubble contracts as the reattachment point approaches the leading edge, and as the shortened bubble encounters the large adverse pressure gradient, it bursts, and a leading-edge vortex commences. The dynamics of the airfoil motion then affect the dynamic stall angle, and the airfoil loads indirectly through their influence on the laminar separation bubble." (Ref. 14, p. 38)

This effect, which is familiarly known as the time lag, can be expressed as a phase lag (between the static and dynamic motions) angle, $\phi = \omega\Delta\tau$, where $\Delta\tau$ is a time constant which is a function of α, $\dot{\alpha}$, $\ddot{\alpha}$, $\bar{\alpha}$, the reduced frequency of oscillation, and the airfoil shape. To evaluate $\Delta\tau$, one has to solve the unsteady boundary equations corresponding to the given dynamic motion of the airfoil; however, at the present time the state of the art of the unsteady boundary layer solutions is inadequate to make such a prediction.

McCroskey (Ref. 19) gave a complete summary of the dynamic stall experimental data and provided a range of ϕ values as functions of $\dot{\alpha}$ and reduced frequencies, which are used to arrive at the ϕ values used in this study. The delay in the separation process is empirically represented by using a prescribed wake obtained from the steady CLMAX program using a modified instantaneous angle of attack, while satisfying the flow boundary conditions in the unsteady flow program corresponding to the instantaneous angle of attack. The modified angle of attack is computed using the expression,

$$\alpha_{mod} = \alpha_m + \bar{\alpha} \sin (\omega t - \phi) \qquad (3.2)$$

where the phase lag, ϕ, is assumed to be a constant throughout a cycle. The value of ϕ can be related to the reduced frequency and $\bar{\alpha}$ for a given airfoil. Although the present model uses a physically consistent model to represent the separation process for steady flow based on a viscous/potential iterative scheme, it does not include the unsteady boundary conditions on the airfoil surface of the effect of the vorticity due to the bursting of the bubble during each cycle.

Numerical Procedure

The unsteady flow computational model is similar to the steady flow model which was described in the previous section. In place of the linearly varying vorticity panels, constant strength doublet panels are used to represent the airfoil surface. For a given instantaneous angle of attack, the separated region is arrived at using the steady flow CLMAX program. A typical grid system with separated wake region is shown in Figure 10. The airfoil is divided into N panels in a clockwise direction along the airfoil surface with panels 1 and N at the trailing edge of the lower and upper surfaces, respectively. The doublet strength, K_i, at any panel, i, is assumed to be a constant across the length of the panel. A cosine grid ($\theta = 0$ to 2π) with a constant angular increment ($\Delta\theta = 2\pi/N$) over each panel is used to fix the panel boundaries (corner points), while the collocation points (where the flow boundary conditions are satisfied) are fixed at $\Delta\theta/2$ from a corner point. The cosine distribution of the grid places more panels near the leading- and trailing-edge regions. From a physical standpoint, this arrangement is good for the representation of the rapidly varying slopes at the leading-edge region and the Kutta condition at the trailing-edge region of the airfoil.

The separation point on the upper surface is always located on a corner point of a panel. This is accomplished by dividing the grid over the upper and lower surfaces into two regions, $0 \leq x \leq x_{sep}$, and $x_{sep} \leq x \leq c$. θ_{sep} is computed using the cosine distribution corresponding to the value x_{sep}, and both regions are divided into a number of panels proportional to their angular distributions. Of course, $\Delta\theta$ may be slightly different in each region, but it provides a smooth distribution of the panels. The upper and lower surfaces are both treated

in this way in order to obtain matched upper and lower panels near the trailing edge--a prerequisite when using piecewise constant doublet panels. This technique proved to be a very effective tool and yielded a smooth pressure distribution.

The flow tangency boundary condition on the airfoil surfaces gives a relation similar to that of Eqn. (3.2) except the kernel on the airfoil surface is the normal velocity due to a unit doublet located on the element, δs, of the line integration. With the assumption of constant strength doublet panels, the integral equation can be reduced into a set of N equations with N unknown values of K_i (for N panels). The physical flow process requires the inclusion of several auxiliary conditions. The first condition is related to the Kutta condition and specifies that the vorticity values at the separation points on the upper and lower surfaces are equal but opposite, and have the values of free vortex sheets (note that the dynamic motion of the wake is neglected), i.e.,

$$\left.\frac{dK}{ds}\right|_{sep} = \left.\frac{dK}{ds}\right|_{lte}, \tag{3.3}$$

where lte is the lower trailing edge. Denoting the separation panel as ISEP, $\left.\frac{dK}{ds}\right|_{sep}$ can be expressed as a function of K_{ISEP}, K_{ISEP-1}, and K_{ISEP-2}; similarly, $\left.\frac{dK}{ds}\right|_{lte}$ can be expressed as a function of K_1, K_2, and K_3. Hence from Equation (3.3), one of the six values amongst K_1, K_2, K_3, K_{ISEP}, K_{ISEP-1} and K_{ISEP-2} can be expressed as a function of the other five values. The second condition concerns the doublet distribution on the airfoil surface in the separation region; this distribution is constrained to start with zero; i.e., $K_{ISEP+1} = 0$, and the

vorticity, $\frac{dK}{ds}$, is made to be zero at the trailing edge by setting $K_N = K_{N-1}$. Now we have eliminated 3 of the N unknowns at N control points. One additional unknown is introduced by distributing a uniform source of unknown strength on the airfoil surface and the two equations satisfying the boundary conditions at panels 1 and N are eliminated due to the symmetric locations of these panels; this procedure did not present any difficulties. Once the doublet distribution is solved for, the vorticity distribution, the pressure distribution, and the loads are computed as explained in the previous section for the steady flow case.

Discussion of the Results

The method was applied to a NACA 0012 airfoil undergoing a sinusoidal motion, $\alpha = 15^0 + 6^0 \sin \omega t$, at a Reynolds number, $R = 6 \times 10^6$. The computations are performed for quasi-steady flow conditions at several instantaneous angles of attack covering the complete range of values of a full cycle. The results are presented for two values of phase angles, $\phi = 30^0$ and 45^0. McCroskey (Ref. 19) presented a comparative study of several empirical formulations for predicting the phase angle for dynamic stall, and concluded that the time constant approach with an average value of 2.82 for $\Delta\tau (= \Delta\tau V_\infty/c)$ provided the most reliable results based on the correlation with the available experimental data. Using this value for

$$\phi = \omega\Delta t = \omega\Delta\tau c/u_\infty = 2k\Delta\tau = 5.64k,$$

where k is the reduced frequency based on the semi-chord length. Using this simple empirical equation, the ϕ values of 30^0 and 45^0 used in this study correspond to the reduced frequencies of 0.0928 and 0.1392, respectively. In reality, the phase lag during the cycle varies. Later in this section an example is presented taking this into account.

The results for C_ℓ versus α and C_m versus α are presented in Figures 11 and 12, respectively. As can be seen from these figures, the results showed typical hysteresis loops that are inherent in the dynamic motion. As expected, the loops are smaller for the smaller value of ϕ, since it corresponds to the lower reduced frequency. The nose-up pitching moment is considered to be positive, and hence, the counterclockwise enclosures of the moment loop are stabilizing while the clockwise enclosures are destabilizing. As can be seen from the moment loops, both cases have net clockwise enclosures, indicating net aerodynamic negative damping. In the present case, the results are not compared with the experimental results since no experimental data is available at the chosen Reynolds number.

The method was also applied to another case, a modified NACA 0012 airfoil undergoing a sinusoidal motion, $\alpha = 15^0 + 10^0 \sin \omega t$, and $k = 0.15$ at a Reynolds number of 2.5×10^6. In Reference 33, an extensive set of experimental data were presented for this particular airfoil and the authors provided us with a detailed computer output for this chosen test case based on 200 equidistant samples per cycle. In order to validate our flow model and the procedure, we felt that it would be desirable to have the detailed experimental data presented in a numerical form as the present case.

In Figure 13, the C_ℓ versus α (experimental) curve for steady flow is shown. We have tried to duplicate this curve by using the steady flow CLMAX program but were unable to do so. The experimental $C_{\ell_{max}}$ is about 15% higher and the authors explained in their report that it may be due to the end wall (wind tunnel) effect. In order to make a valid comparison for the case of an oscillatory motion, we felt that we really need to duplicate this curve for steady flow. Hence, the separated wake geometry is adjusted in such a way that the experimental curve is duplicated and the following procedure is adopted:

(i) The steady flow CLMAX program is used to compute x_{sep}, and the wake axial (along the x-axis) locations are a function of α.

(ii) The unsteady flow program is used to iterate on the height of the wake intersection point to obtain a C_ℓ corresponding to the experimental value for each α in the complete range of 5^0 to 25^0.

(iii) The wake geometry obtained in (ii) is used in the unsteady flow analysis.

The comparison of C_ℓ versus α between the experimental and the computed results for two constant phase angles are shown in Figure 14. As can be seen from this figure, the attained peak values for C_ℓ = 2.2 and 2.64, for $\phi = 45^0$ and 75^0, respectively, while the experimental peak is about 3.0. Also at higher values of ϕ, C_ℓ decreases rather rapidly during the deceleration phase of the cycle (decreasing angles of attack) going through even negative values (the full cycle is not shown here). The reason for this is at the chosen high value of $\phi(=75^0)$, the separation point location on the upper surface of the airfoil continues to move more and more forward towards the leading edge as the angle of attack decreases, resulting in a greater loss of lift. Admittedly, this representation of a constant ϕ is a gross oversimplification for representing such a complex phenomenon; however, it is felt that this example helps in understanding the physical process involved. From this example, it is obvious that one has to use a variable distribution (i.e., an appropriate phase lag variation) during a cycle for the proper representation of the dynamic stall.

Figure 15 gives the required ϕ distribution to duplicate the experimental curve (solid line). In the region near the stall (α is about 25^0), it is really not possible to obtain the appropriate peak value of C_ℓ without including the effects of the wake dynamics and the passage of the leading-

edge vortex over the upper surface of the airfoil. The dotted line in the figure is arrived at by using the following simple concept. The phase lag angle, ϕ, is assumed to vary in a linear fashion in the range, $15^0 < \alpha < 25^0$. However, during the decreasing angle-of-attack range, an additional restriction is imposed. The separation point location on the upper surface is not permitted to move beyond a fixed forward location and the appropriate ϕ is chosen, satisfying this condition. This restriction enables the maintainance of adequate lift during the decreasing angle of attack portion of the cycle. The phase angle is fixed at 45^0 during the remaining portion of the cycle, $5^0 < \alpha < 15^0$. As can be seen from the figure, this simple concept results in a reasonable representation of the dynamic stall process.

Discussion on Leading-Edge Separation

The dynamic stall model so far in this section is applicable for a trailing-edge separation problem, which is the typical case for airfoils of moderate thickness. It is felt that it is appropriate to include a brief discussion on the leading-edge separation under dynamic conditions and an analysis method for predicting the onset of leading-edge separation is presented here.

In Reference 34, a correlation of leading-edge stall provided a criterion for the maximum leading-edge velocities that can be sustained and is used to indicate the initiation of the separation process, i.e., leading-edge vortex shedding. For a set of airfoils, which under quasi-steady conditions exhibit an abrupt stall, Evans and Molt (Ref. 34) have computed the velocity distribution and obtained correlation between the maximum obtainable peak velocity and a parameter idealizing the adjacent adverse gradient. Applicability is limited by the requirement of a sufficiently high value of the local Reynolds

number based on the laminar boundary layer momentum thickness. For many practical airfoils, maximum lift is limited by trailing-edge separation under static conditions so that the leading edge never achieves the high local velocity appropriate to the leading-edge stall. Under dynamic conditions, however, trailing-edge separation is delayed, as discussed earlier in this section, and so, depending on the rate of increase of angle of attack, the leading edge may become critical according to the above correlation.

In a recent paper (Ref. 35), the above criterion has been applied to predict the onset of airfoil separation under dynamic conditions. The instantaneous (time-dependent) chordwise velocity distribution is computed by using more exact potential flow methods for attached flow conditions. The information is used to predict the limit of attached flow or, alternatively, the initiation of the separation.

A potential unsteady flow program applicable to thick airfoils is developed and is checked out against Theodorsen's results in the limiting case of zero thickness thin airfoils. From this program, the chordwise velocity distribution can be computed from which the separation phenomenon can be investigated making use of the criterion given in Reference 34. However, at the present time, this program is not completely checked out; when it is, it can be incorporated into the dynamic stall program as an independent subroutine. Then the dynamic stall program will have the capability to treat either the leading edge or the trailing edge separation problem.

IV. CONCLUSIONS AND FURTHER APPLICATIONS

The steady flow CLMAX program employs a realistic wake model for separated flow. The wake model uses free vortex sheets to separate the free stream from the wake region. The method has generated accurate C_ℓ versus α curves for several airfoils up to and beyond the stall at a cost of about $12 per incidence data point--a mere fraction of the cost of manufacturing and testing a model. The calculation provides the complete pressure distribution, including pressures in the separated region at each data point as well as the force and moment values. Lift, pitching moment, and pressure distribution comparisons between calculated and experimental results for several airfoil sections is excellent. There is very good agreement even in the separated flow region where the vortex model allows pressures to be calculated directly.

The steady flow analysis and the computer program have been accepted by the scientific community as one of the most powerful and practical engineering tools for predicting the flow over two-dimensional airfoils at higher angles of attack. The computer program is being currently used by the Sikorsky, Hughes Helicopter and Beech Aircraft companies. Several scientists at the Fort Eustis, Langley and Ames Directorates of the USAAMRDL and also the NASA Ames and Langley Research Centers are using the compuer programs.

An analysis and a computer program for predicting a typical trailing-edge induced separation process of a two-dimensional airfoil undergoing pitching oscillations are developed. A quasi-steady approach is used to solve the flow field at several angles of attack during a complete cycle. The separation wake used is computed from the steady flow program and is modified

in a semi-empirical fashion to include the phase lag effect at each of the selected angle-of-attack range of the cycle. The wake model and the separation region do not include the effects of the dynamic motion and the laminar bursting process. Limited comparisons between computed and experimental results of C_ℓ versus α look promising in spite of the simplifying assumptions. However, additional improvements, such as the inclusion of the unsteady boundary layer effects and wake dynamics are essential before this method can be established as a practical engineering tool for predicting the dynamic stall process.

A brief discussion on the criterion for predicting the onset of leading-edge separation under dynamic conditions is included. The chordwise velocity distribution, especially the peak velocity near the leading-edge, plays a major role in the leading-edge separation process under dynamic conditions. A computer program for predicting the chordwise velocity distribution over two-dimensional airfoils under unsteady attached flow conditions is developed. When this program is fully checked out, it can be incorporated into the dynamic stall program as an independent subroutine, thereby providing the program with the additional capability of dealing with the leading-edge as well as the trailing-edge separation process.

Further Applications

The development of the two-dimensional separation flow models under the present contract provided the technical background and tools for further development of separated flows. At the present time, Analtyical Methods, Inc. is involved with the development of several research programs, direct extensions of the present work, under contract with several governmental agencies, some of which are listed below:

(i) "Prediction of Aerodynamic Characteristics of Fighter Aircraft at High Lift", (Contract sponsored by the Office of Naval Research).

Development of a basic viscous/potential iterative technique for calculating the flow on finite wings up to and beyond the stall.

(ii) "An Anlysis Method for Multi-Component Airfoils in Separated Flows", (Contract sponsored by the NASA Langley Research Center).

Inclusion of the two-dimensional separation flow model in the Multi-Component Airfoil Analysis Program (MCARF) developed by NASA Langley Research Center and Lockheed Aircraft Company.

(iii) "Unsteady Flow Model for Circulation-Control Airfoils", (Contract Sponsored by the NASA Ames Research Center).

Development of an approximate procedure to represent the physical flow model for circulation-control airfoils.

V. REFERENCES

1. Jacob, K., "Computation of Separated Incompressible Flow Around Airfoils and Determination of Maximum Lift", AVA Report 67, A, 62, 1967.

2. Bhateley, I.C. and McWhirter, J.W., "Development of Theoretical Methods for Two-Dimensional Multi-Element Airfoil Analysis and Design, Part I: Viscous Flow Analysis Method", Technical Report AFFDL-TR-72-96, 1972.

3. Woodward, F.A., Dvorak, F.A. and Geller, E.W., "A Computer Program for Three-Dimensional Lifting Bodies in Subsonic Inviscid Flow", USAAMRDL Technical Report 74-18, Flow Research Report No. 26, Prepared for the Eustis Directorate, U.S. Air Mobility Research and Development Laboratory, Ft. Eustis, Virginia, April 1974.

4. Halfman, R.F., Johnson, H.C. and Haley, S.M., "Evaluation of High Angle-of-Attack Aerodynamic Derivative Data and Stall Flutter Prediction Techniques", NACA TN 2533, 1951.

5. Carta, F.O., "Experimental Investigation of the Unsteady Aerodynamic Characteristics of a NACA 0012 Airfoil", United Aircraft Research Labs. Report, M-1283-1, August 1960.

6. Windsor, R.I., "Measurements of Aerodynamic Forces on an Oscillating Airfoil", USAAVLABS TR 69-98, 1969.

7. Liiva, J., "Unsteady Aerodynamic Stall Effects on Helicopter Rotor Blade Airfoil Section", J. Aircraft, Vol. 6, No. 1, 1969, pp. 46-51.

8. Liiva, J., Davenport, F.J., Gray, L., and Walton, I.C., "Two-Dimensional Tests of Airfoils Oscillating Near Stall", USAAVLABS TR 68-13, 1968.

9. Martin, J.M., Empey, R.W., McCroskey, W.J. and Carodona, F.X., "An Experimental Analysis of Dynamic Stall on Oscillating Airfoils", J. Am. Hel. Soc., Vol. 19, No. 1, January 1974, pp. 26-32.

10. McCroskey, W.J., Carr, L.W., and McAlister, K.W., "Dynamic Stall Experiments on Oscillating Airfoils", AIAA Paper No. 75-125, 1975.

11. Ham, N.D., "Aerodynamic Loading on a Two-Dimensional Airfoil during Dynamic Stall", AIAA J., Vol. 6, No. 10, October 1968, pp. 26-33.

12. Liiva, J. and Davenport, F.J., "Dynamic Stall of Airfoil Sections for High-Speed Rotors", J. Am. Hel. Soc., Vol. 14, No. 2, April 1969, pp. 26-33.

13. Ericksson, L.E. and Reding, J.P., "Dynamic Stall of Helicopter Rotor Blades", J. Am. Hel. Soc., Vol. 17, No. 1, January 1972, pp. 11-19.

14. Johnson, W. and Ham, N.D., "On the Mechanism of Dynamic Stall", J. Am. Hel. Soc., Vol. 17, No. 4, October 1972, pp. 36-45.

15. Carta, F.O., Commerford, G.L. and Carlson, R.G., "Determination of Airfoil and Rotor Blade Dynamic Stall Response", J. Am. Hel. Soc., Vol. 18, No. 2, April 1973, pp. 31-39.

16. Crimi, P. and Reeves, B.L., "A Method for Analysing Dynamic Stall", AIAA Paper No. 72-37, January 1972.

17. Shamroth, S.J. and Kreskovsky, J.P., "A Weak Interaction Study of the Viscous Flow About Oscillating Airfoils", NASA CR 132425, May 1974.

18. Mehta, U.B., "Dynamic Stall of an Oscillating Airfoil", Presented at the AGARD Fluid Dynamics Panel Symposium on Unsteady Aerodynamics, AGARD-CP-227, Paper No. 23, September 1977.

19. McCroskey, W.J., "Recent Developments in Dynamic Stall", Proceedings of a Symposium held at the University of Arizona on Unsteady Aerodynamics, Vol. I, July 1975, pp. 1-33.

20. McCroskey, W.J., "Some Durrent Research in Unsteady Fluid Dynamics", J. Fluid Engr., Vol. 99, March 1977, pp. 8-38.

21. Maskew, B. and Dvorak, F.A., "An Investigation of Separation Models for the Prediction of $C_{\ell_{max}}$", Interim Technical Report 1, U.S. Army Research Office, Contract DAAG29-76-C-0019, June 1976.

22. Maskew, B. and Dvorak, F.A., "An Investigation of Separation Models for the Prediction of $C_{\ell_{max}}$", Interim Technical Report 2, U.S. Army Research Office, Contract DAAG29-76-C-0019, December 1976.

23. Maskew, B. and Dvorak, F.A., "An Investigation of Separation Models for the Prediction of $C_{\ell_{max}}$", Interim Technical Report 3, U.S. Army Research Office, Contract DAAG29-76-C-0019, June 1977.

24. Maskew, B. and Dvorak, F.A., "The Prediction of $C_{\ell_{max}}$ Using a Separated Flow Model", J. Am. Hel. Soc., April 1978.

25. Rao, B.M., Maskew, B.M., and Dvorak, F.A., "Theoretical Prediction of Dynamic Stall on Oscillating Airfoils", Presented at the 34th Annual National Forum of the American Helicopter Society, Preprint No. 78-62, May 1978.

26. Curle, H., "A Two-Parameter Method for Calculating the Two-Dimensional Incompressible Boundary", J. R. Aero. Soc. Vol. 71, 1967.

27. Thwaites, B., "Approximate Calculation of the Laminar Boundary Layer", Aero. Quart., Vol. I, 1949.

28. Kline, S.J., Morkovin, M.V., Sorran, G., and Cockrell, D.J., "Computation of Turbulent Boundary Layers", Proceedings 1968 AFOSR-IFP Stanford Conference, Stanford University, Stanford, California, 1969.

29. Nash, J.F. and Hicks, J.G., "An Integral Method Including the Effect of Upstream History on the Turbulent Shear Stress", Proceedings of Computation of Turbulent Boundary Layers--1968 AFOSR-IFP Stanford Conference, Vol. 1, Stanford University Department of Mechanical Engineering, Stanford, California.

30. Dvorak, F.A., "The Calculation of Turbulent Boundary Layers on Rough Surfaces in Pressure Gradient", AIAA J., Vol. 7, No. 9, September 1969.

31. Dvorak, F.A., "The Calculation of Compressible Turbulent Boundary Layers with Roughness and Heat Transfer", AIAA J., Vol. 10, No. 11, November 1972.

32. Pinkerton, R.N., "The Variation with Reynolds Number of Pressure Distribution over an Airfoil Section", NACA Report No. 613.

33. McAlister, K.W., Can, L.W., and McCroskey, W.J., "Dynamic Stall Experiments on the NACA 0012 Airfoil", NACA Technical Paper 1100, January 1978.

34. Evans, W.R. and Mort, K.W., "Analysis of Computed Flow Parameters for a Set of Sudden Stalls in Low Speed Two-Dimensional Flow", NASA TN D-85, 1959.

35. Beddoes, T.S., "Onset of Leading-Edge Separation Effects under Dynamic Conditions and Low Mach Number", Presented at the 34th Annual National Forum of the American Helicopter Society, May 1978.

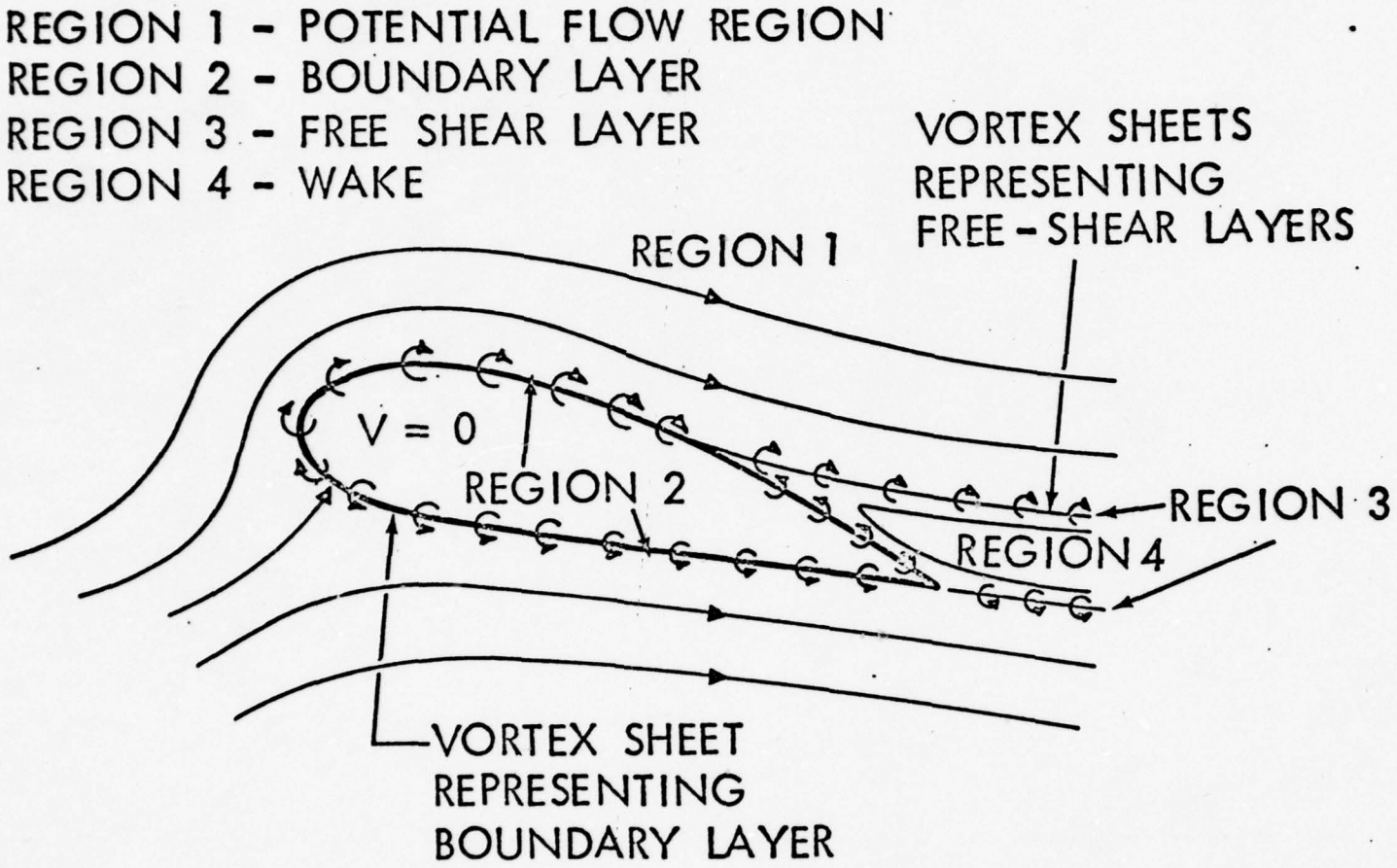

Figure 1. Mathematical Flow Model.

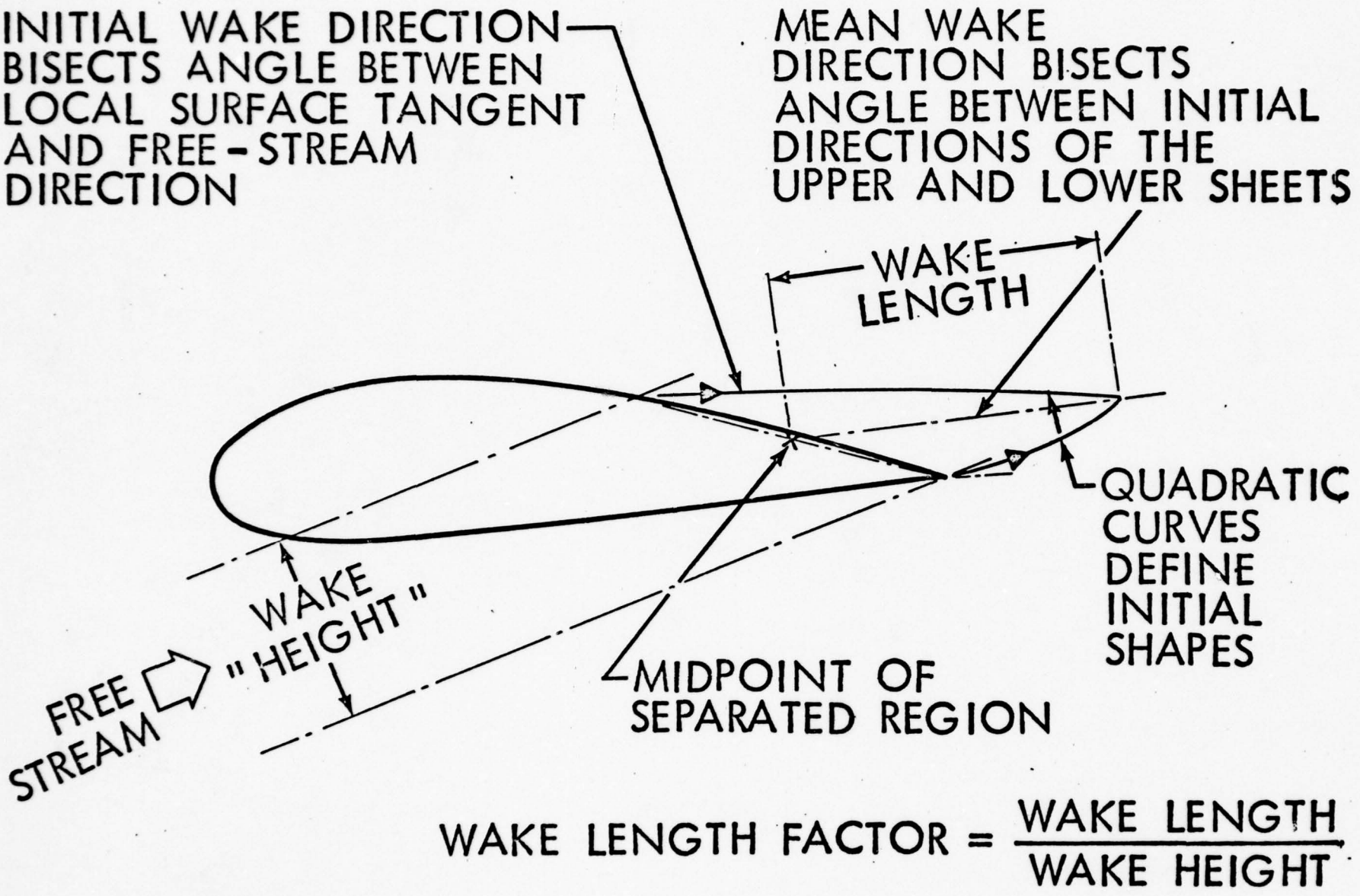

Figure 2. Initial Wake Geometry.

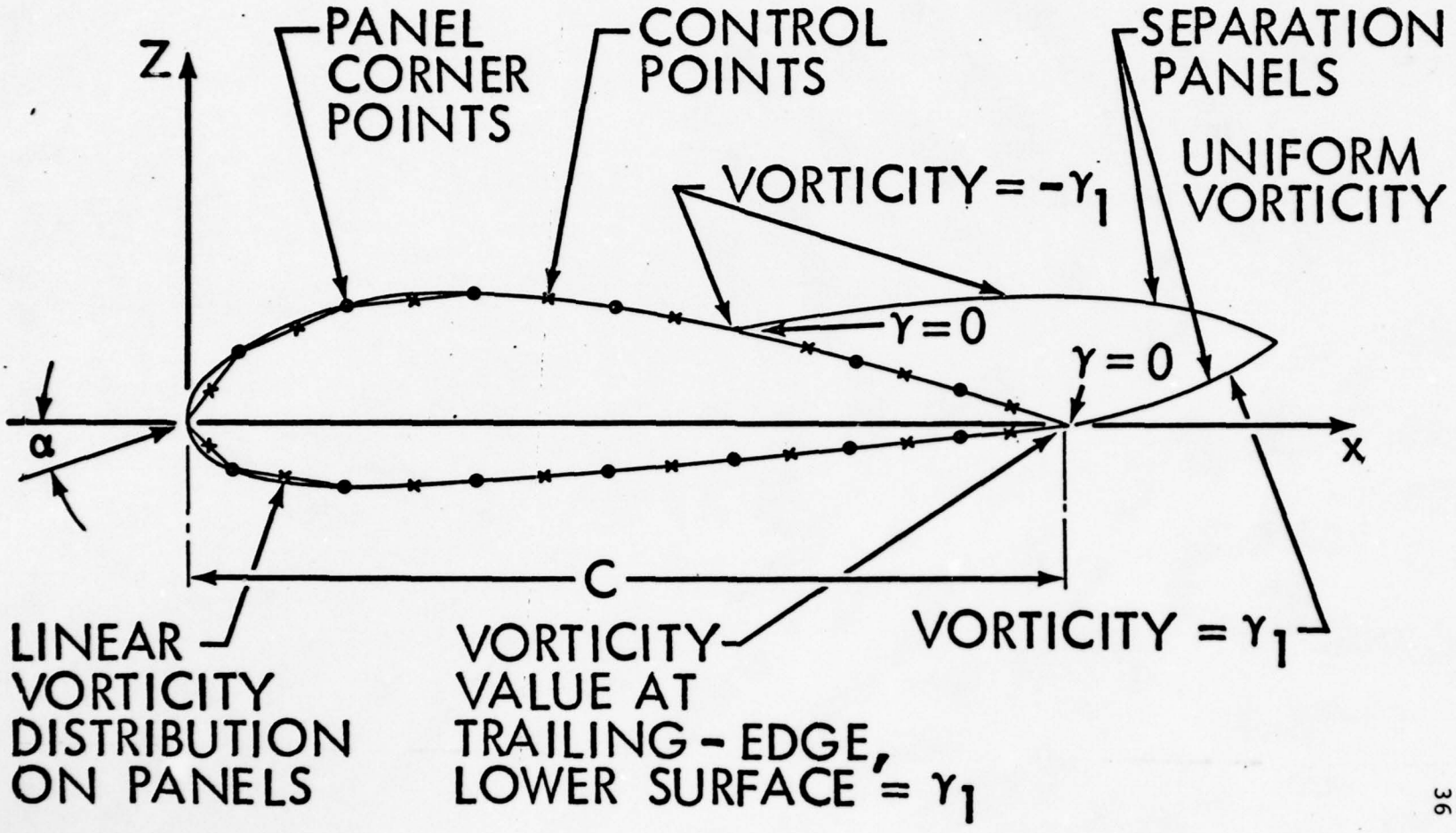

Figure 3. Vorticity Model for the Potential Flow.

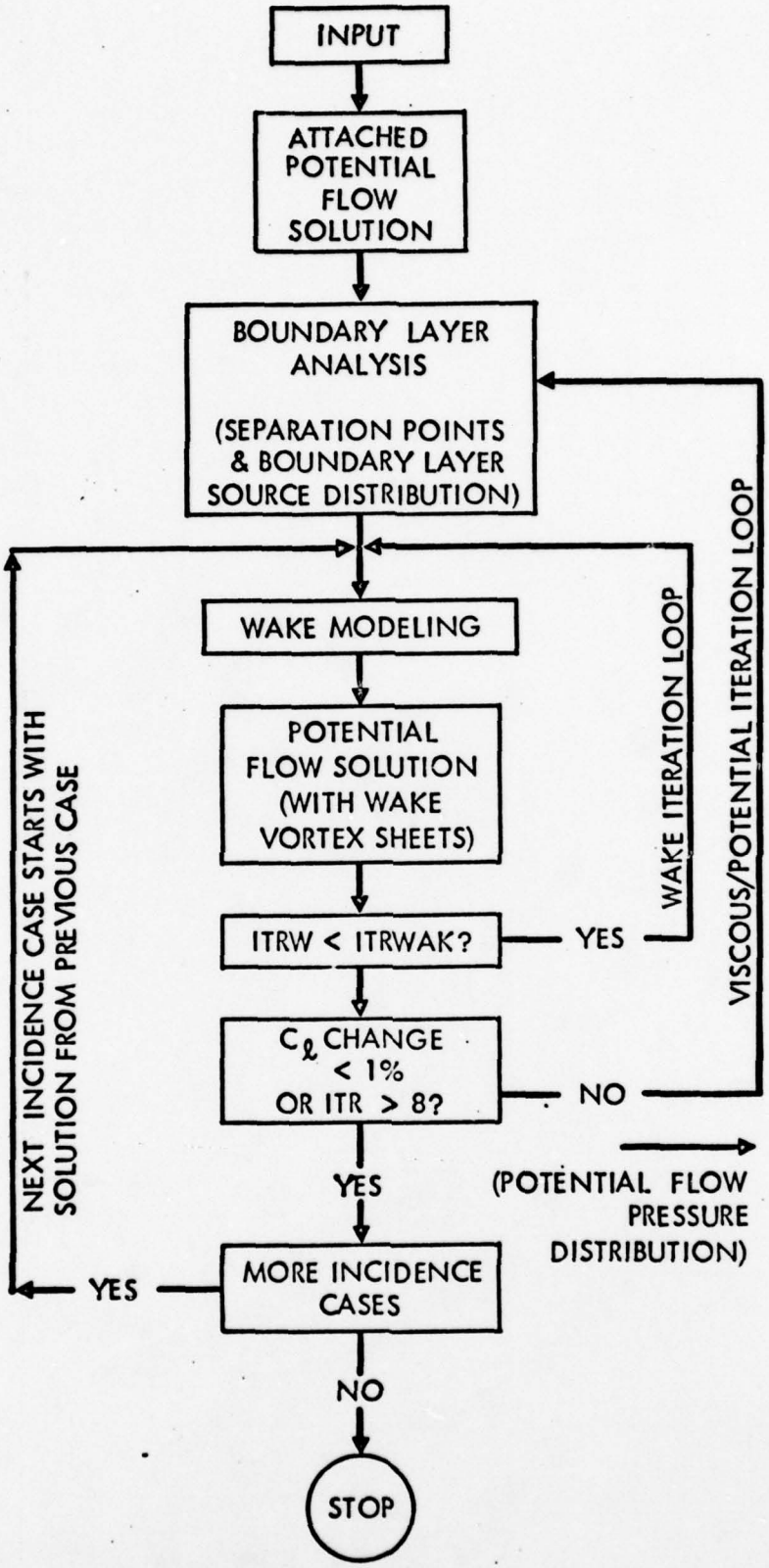

Figure 4. Program Outline.

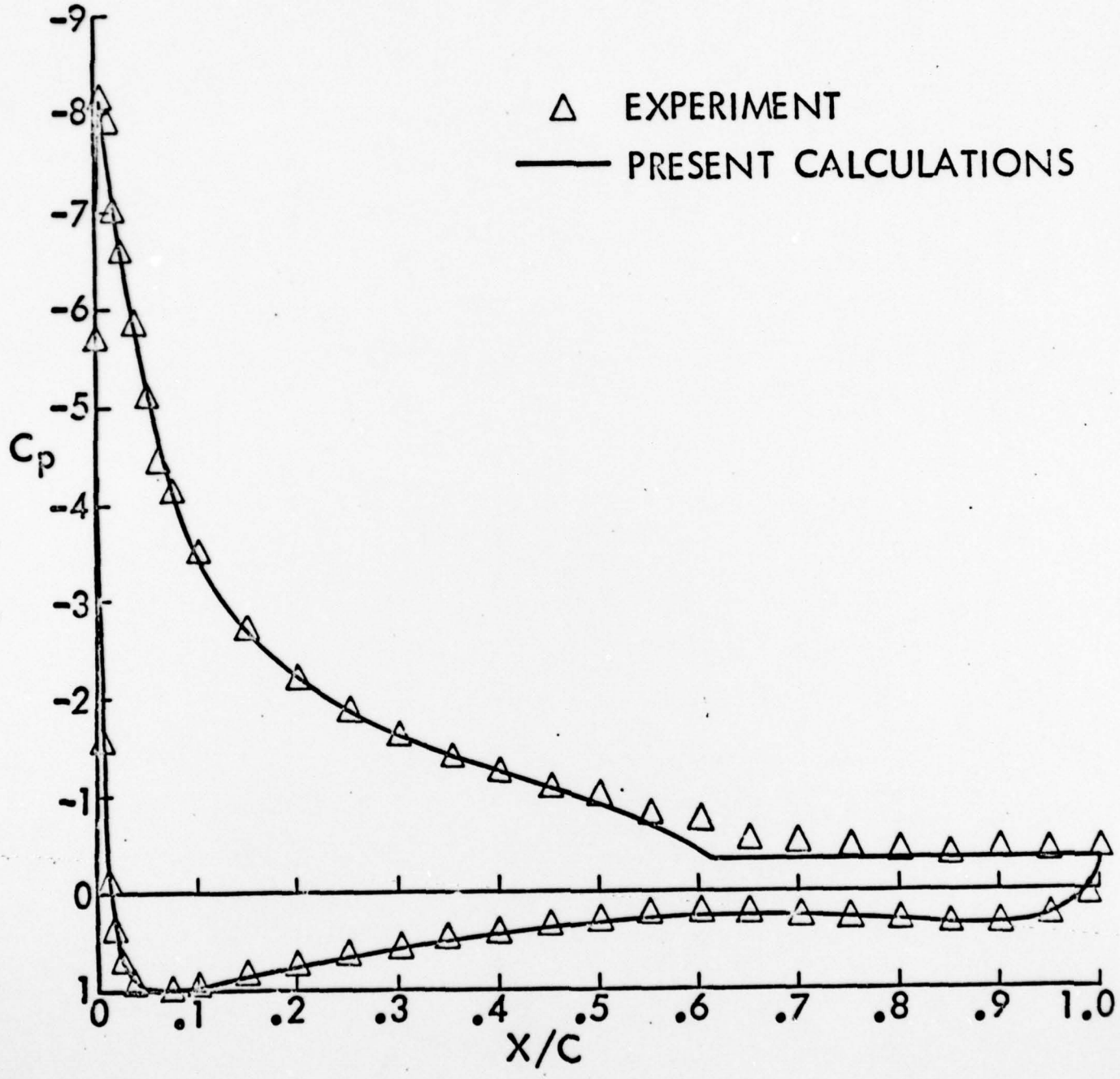

Figure 5. Comparison of Calculated and Experimental Pressure Distributions on a GA(W)-1 Airfoil at $C_{\ell_{max}}$. Incidence = 19.06^0; Re = 6.3×10^6.

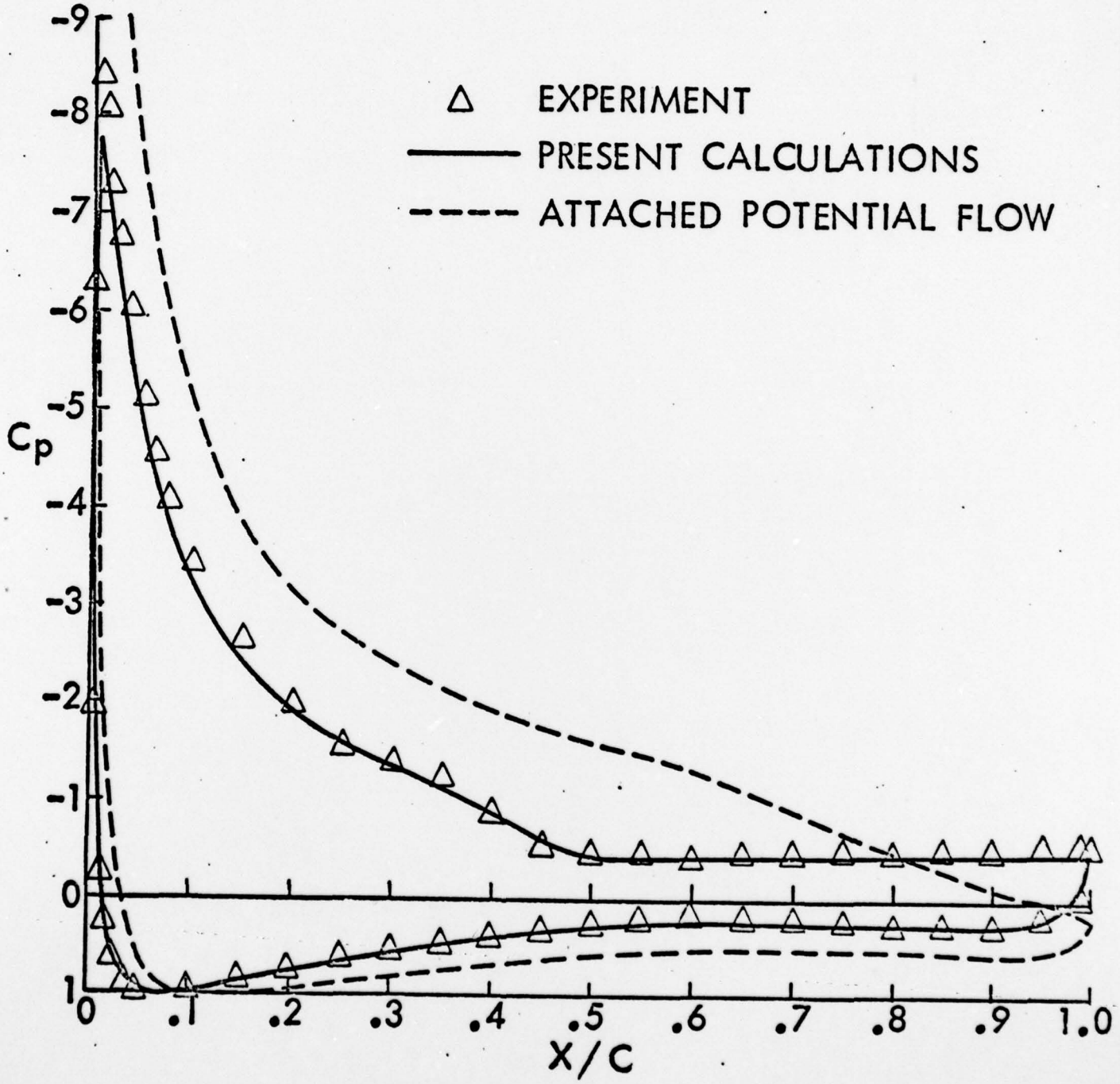

Figure 6. Comparison of Calculated and Experimental Pressure Distributions on a GA(W)-1 Airfoil Post Stall: $Re = 6.3 \times 10^6$.

(a) Incidence = 20.05^0.

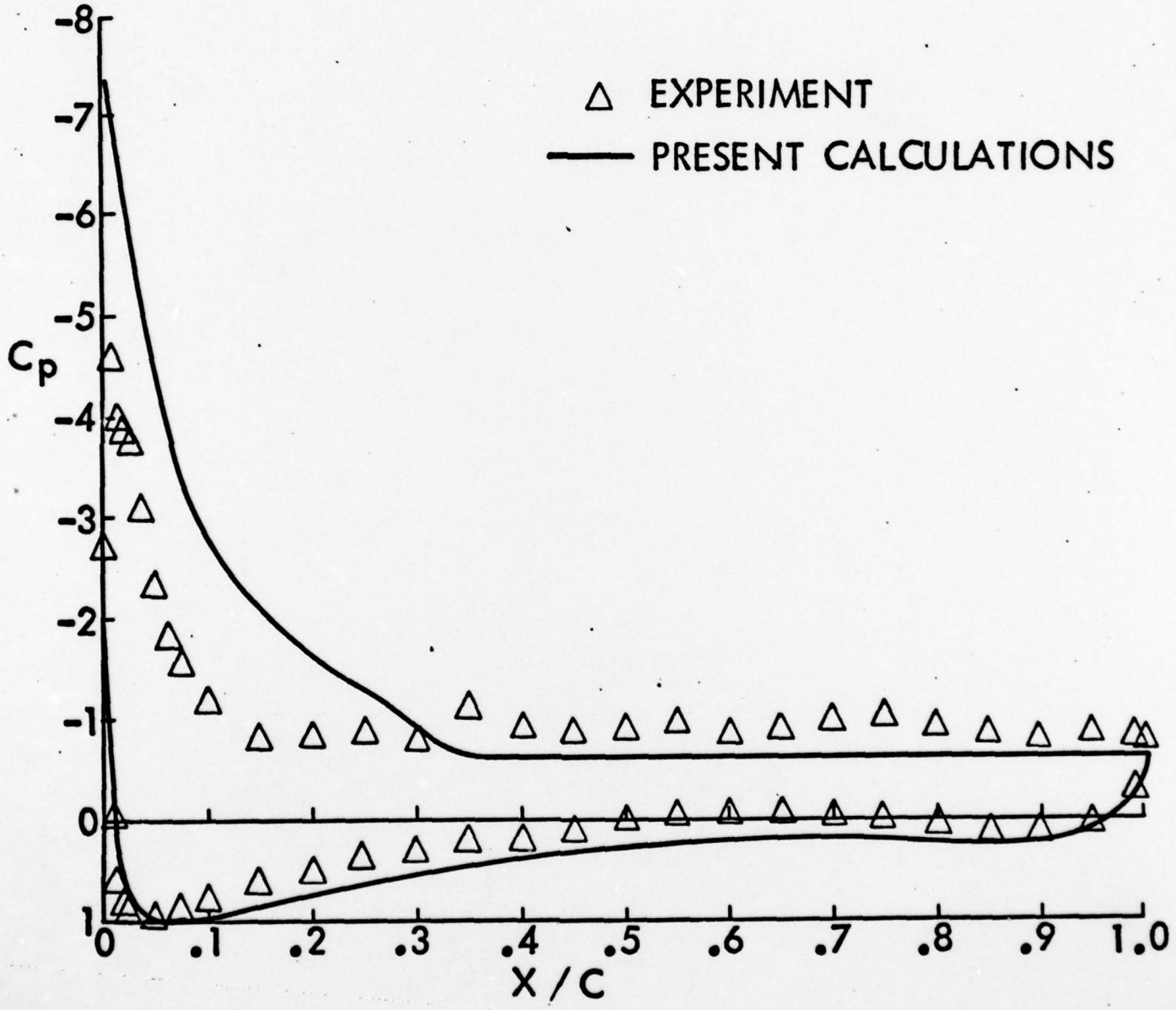

Figure 6. Concluded.

(b) Incidence = 21.14^0.

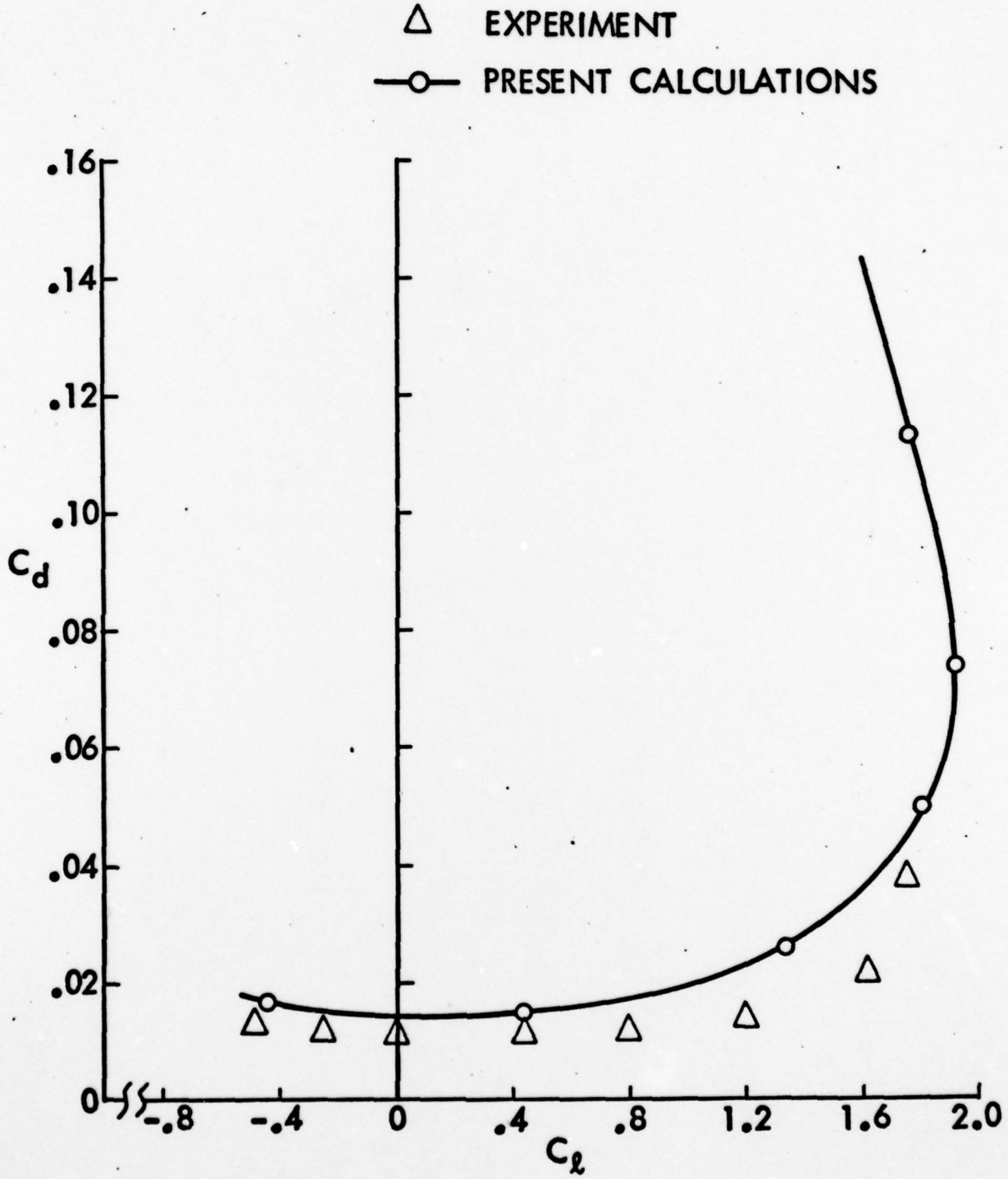

Figure 7. Comparisons of Calculated and Experimental Drag Characteristics for the GA(W)-1 Airfoil: Re = 6.3 x 10^6.

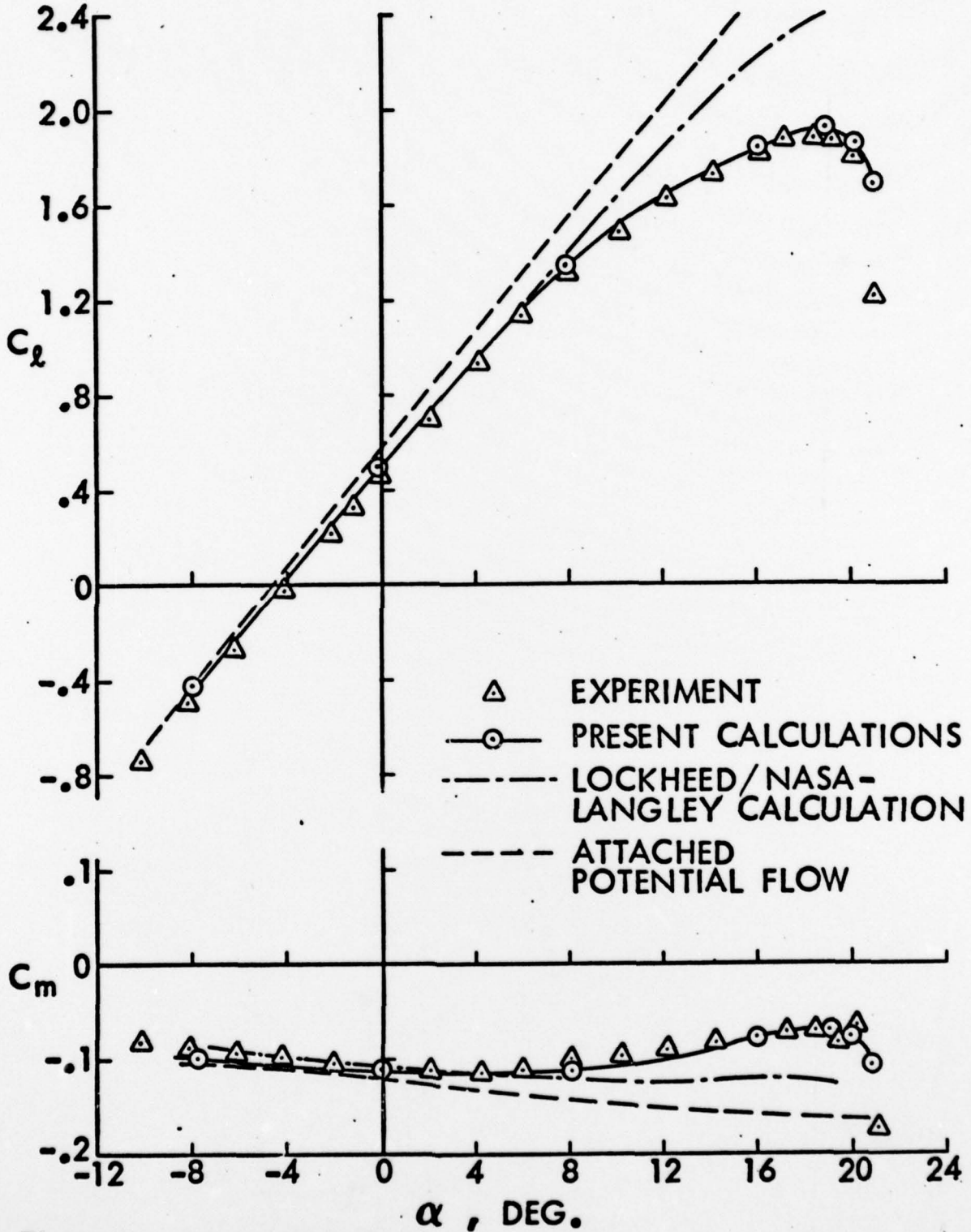

Figure 8. Comparisons of Calculated and Experimental Lift and Pitching Moment Characteristics for the GA(W)-1 Airfoil.
(a) Reynolds Number = 6.3×10^6.

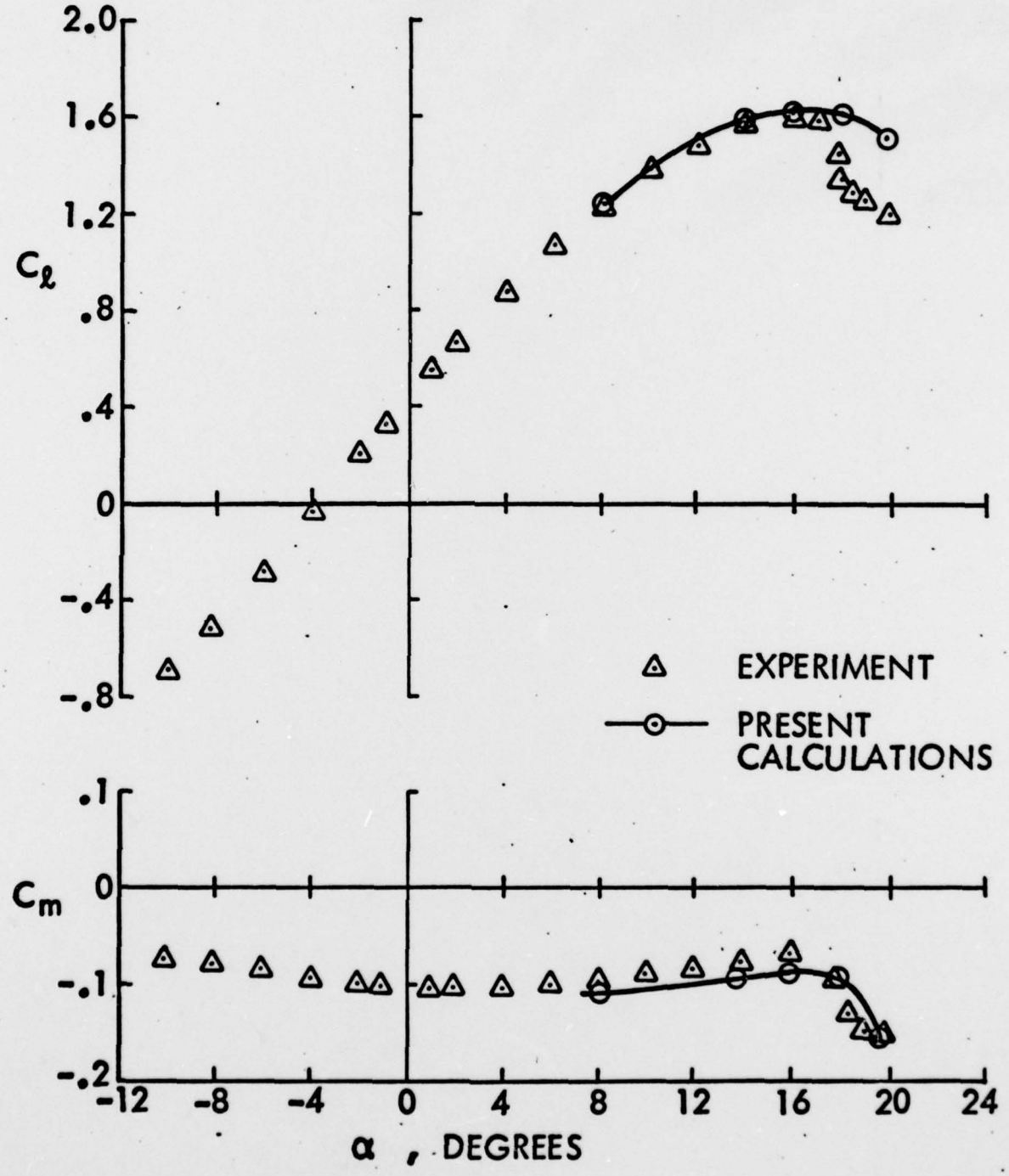

Figure 8. Concluded.

(b) Reynolds Number = 2.1×10^6.

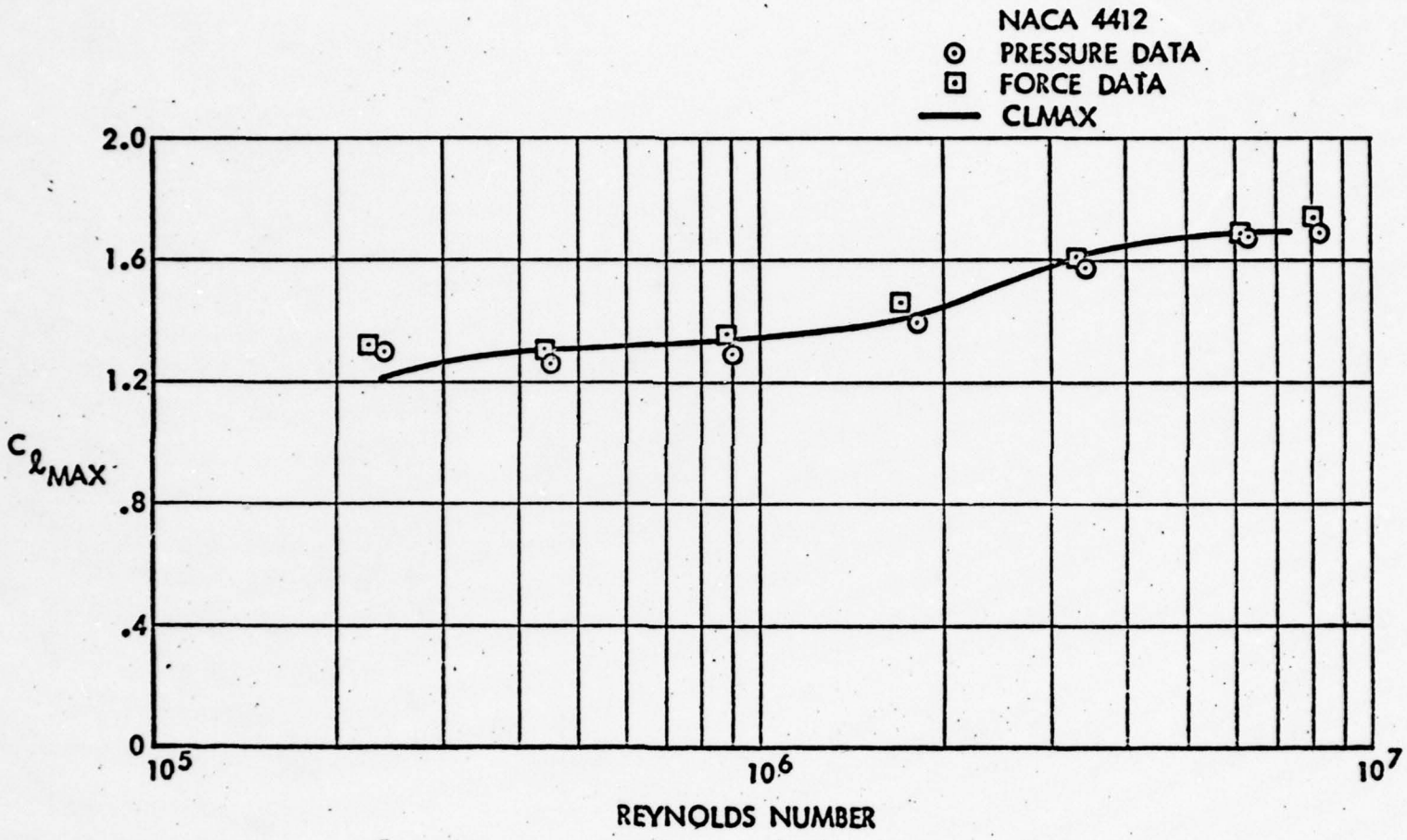

Figure 9. Comparison of Calculated and Experimental $C_{\ell_{max}}$ Variation with Reynolds Number for the NACA 4412 Airfoil.

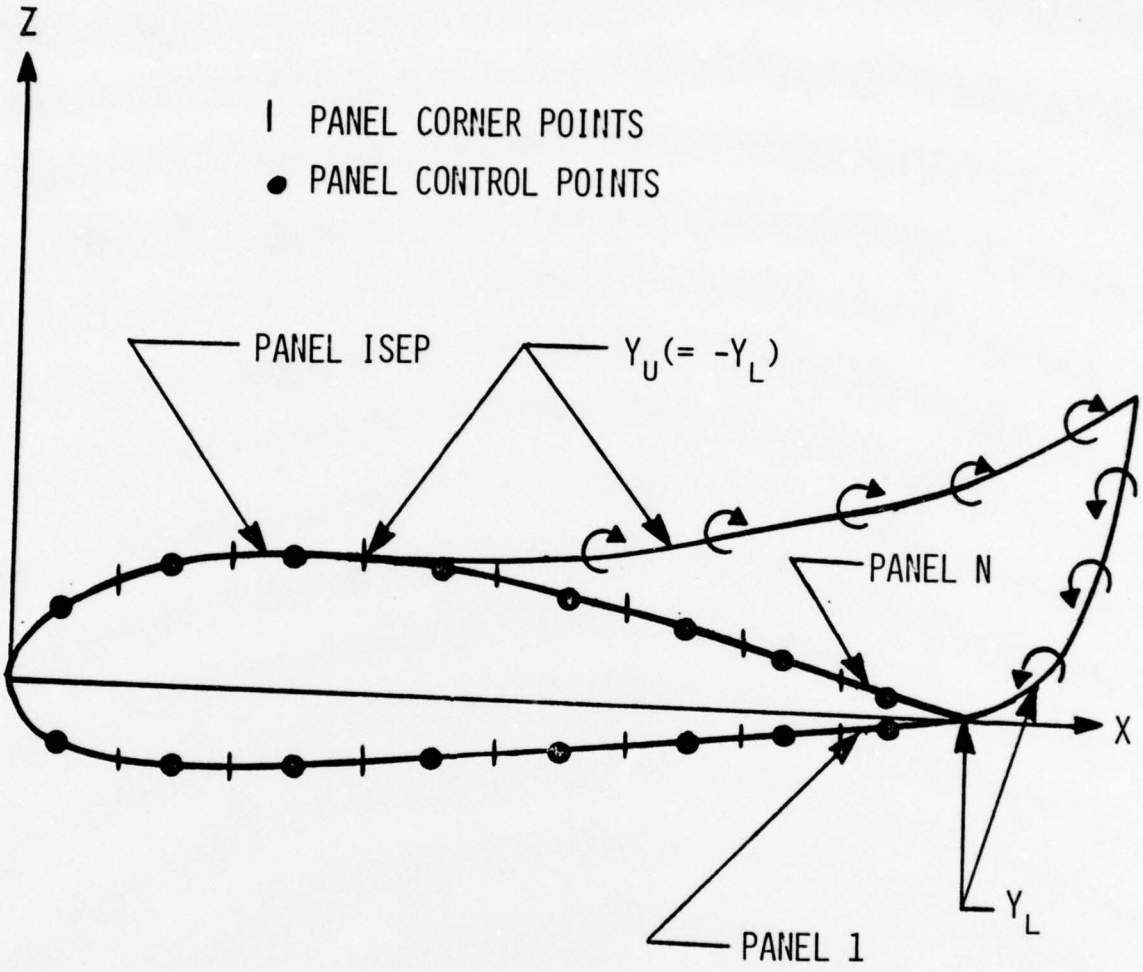

Figure 10. Panel Representation of the Airfoil Surface and Separated Region.

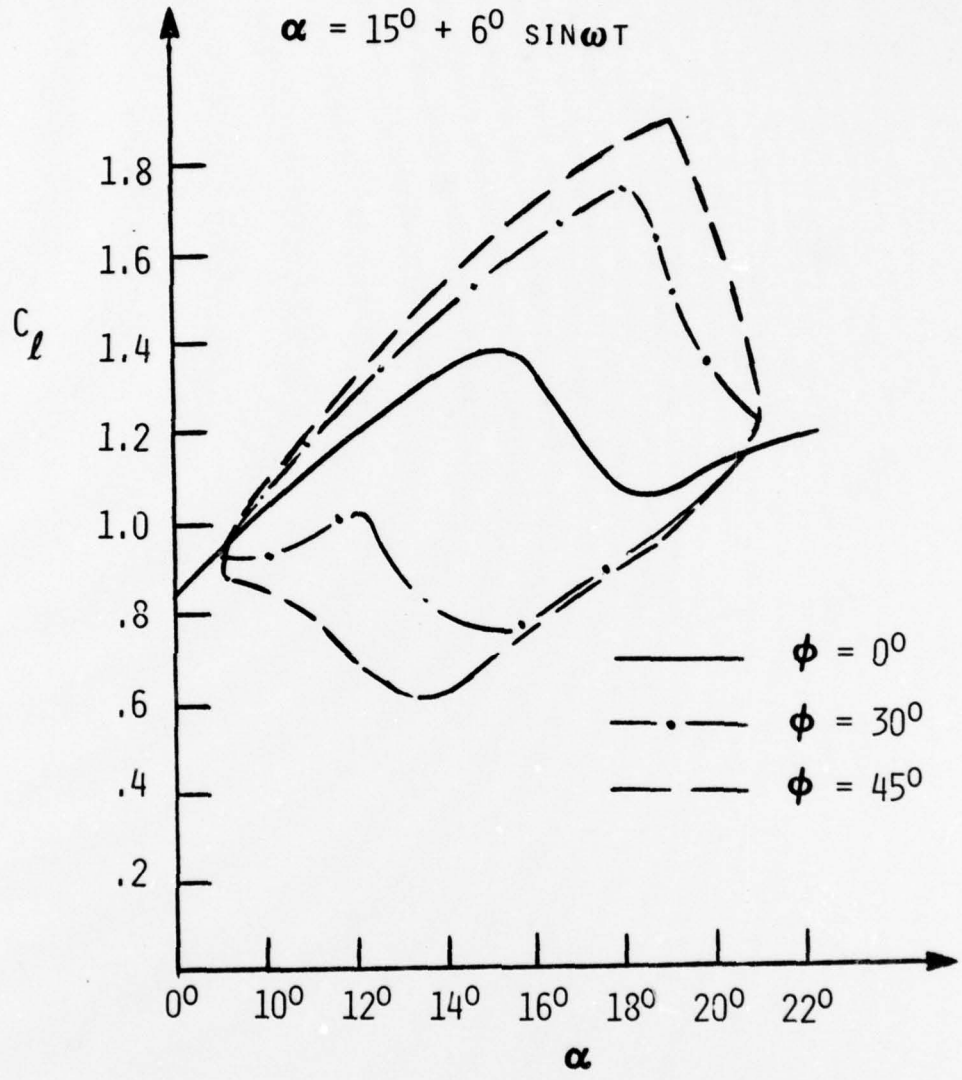

Figure 11. C_ℓ Versus α (NACA 0012).

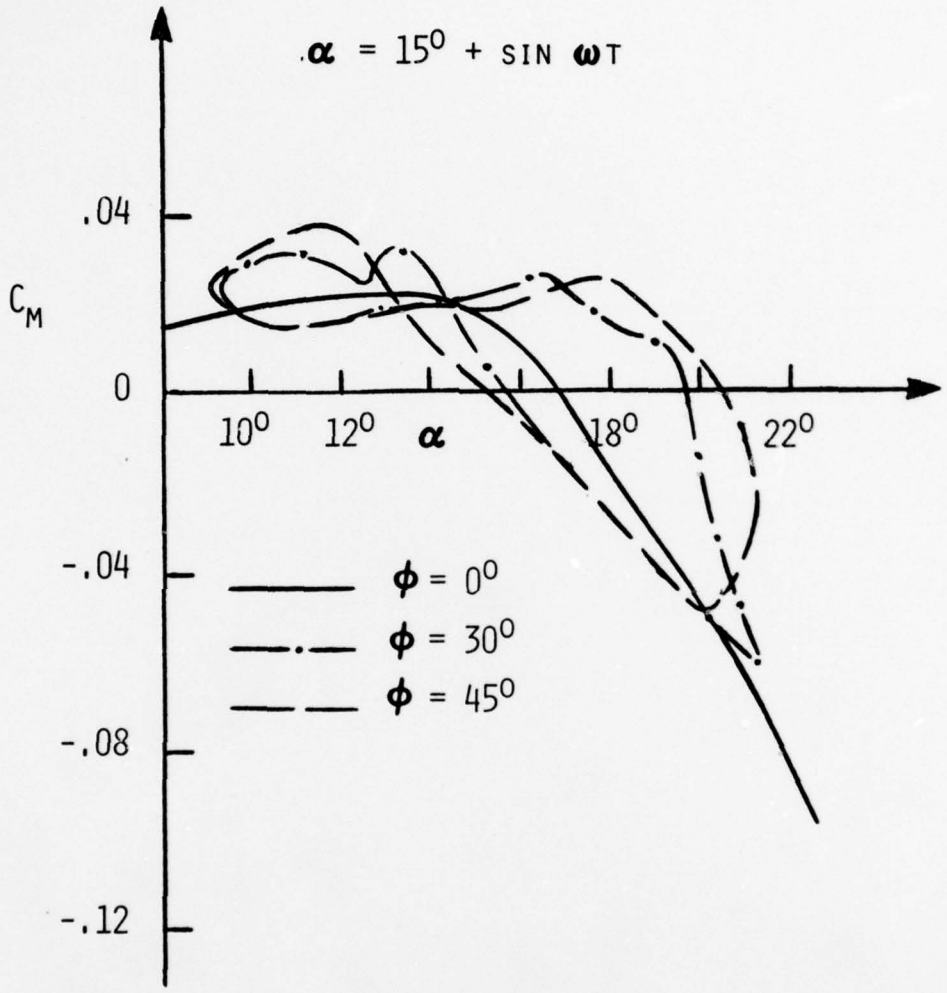

Figure 12. C_m Versus α (NACA 0012 Airfoil).

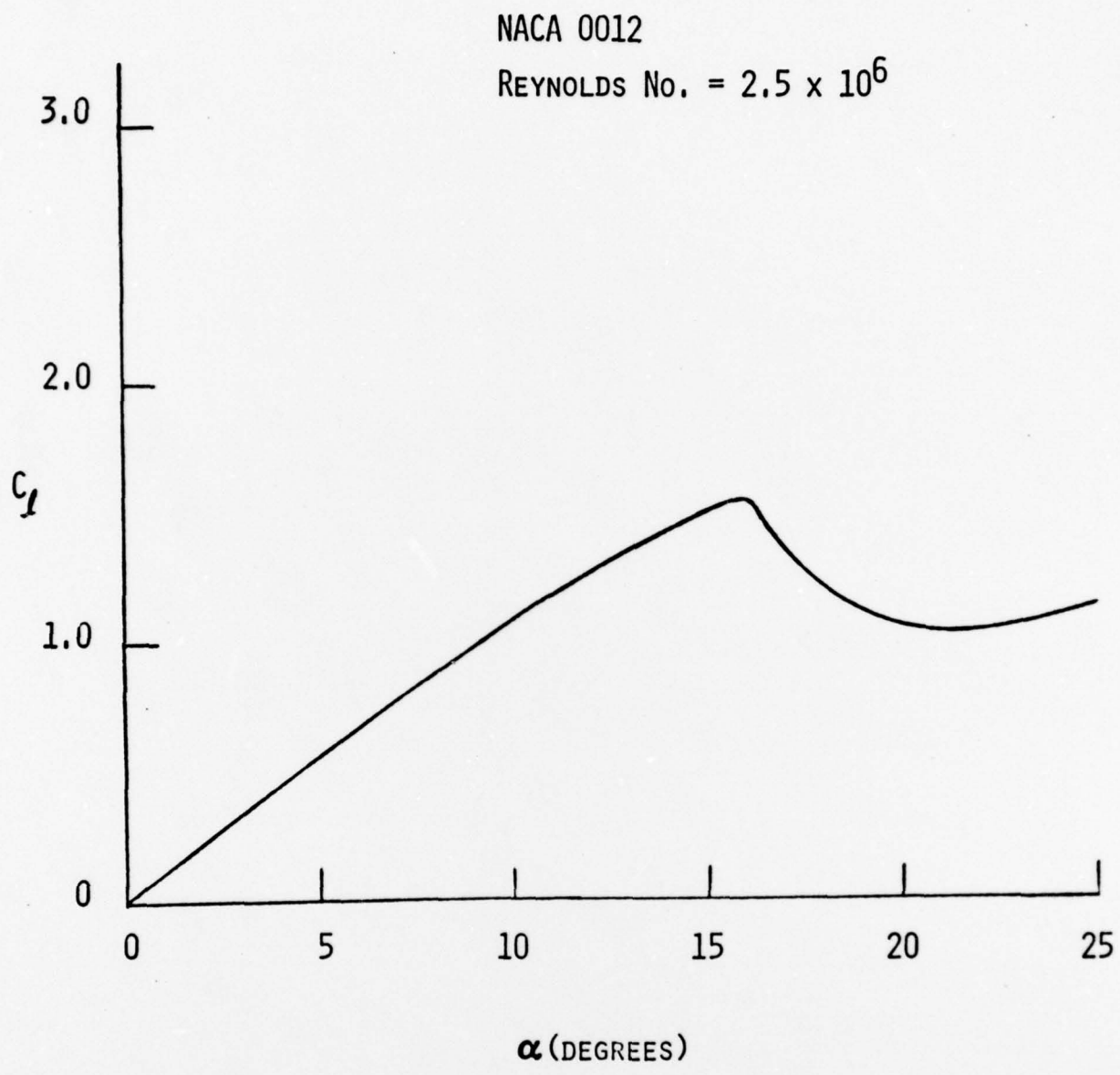

Figure 13. C_ℓ Versus α (Experiment).

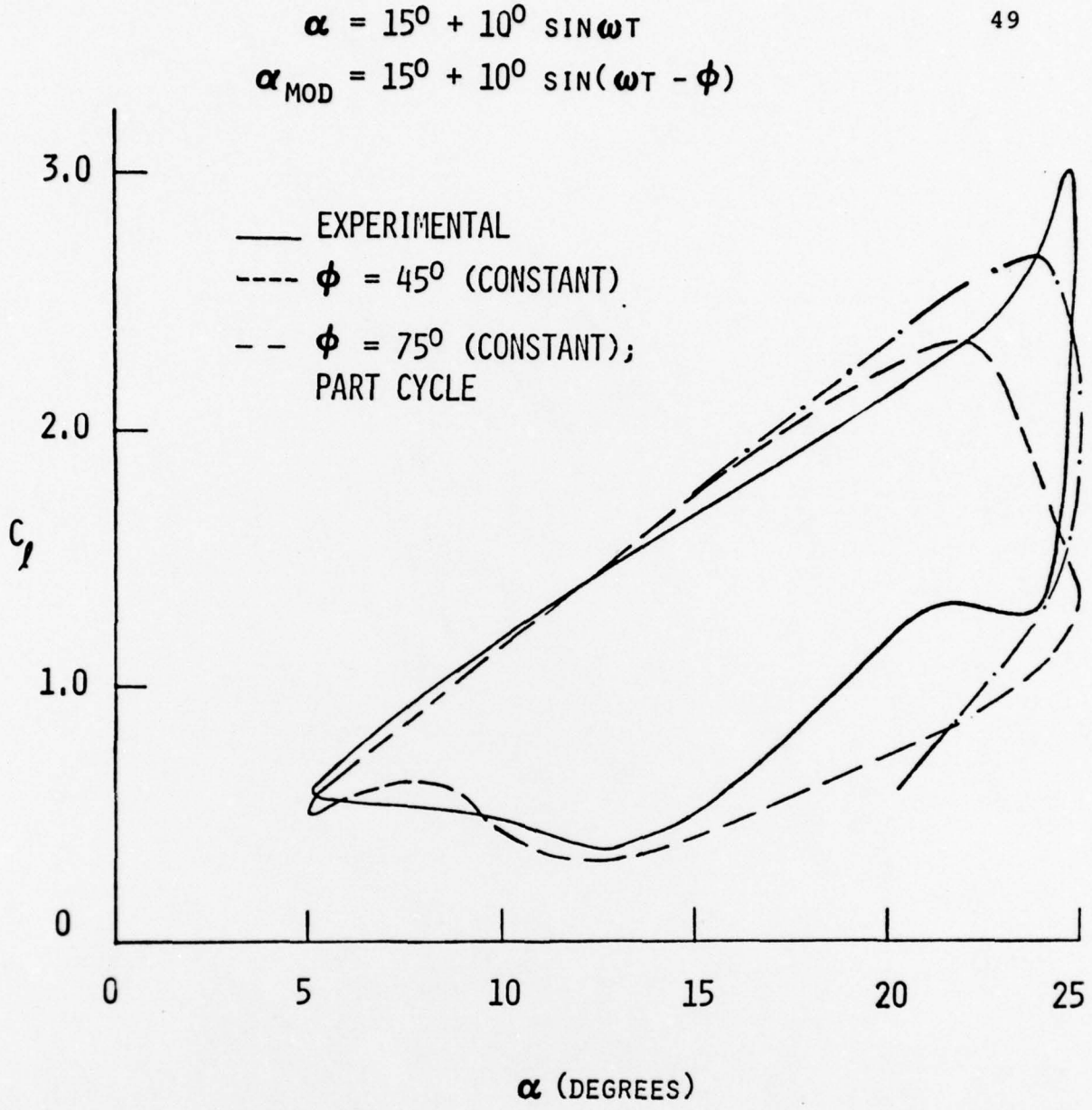

Figure 14. C_ℓ Versus α - Oscillatory Motion.

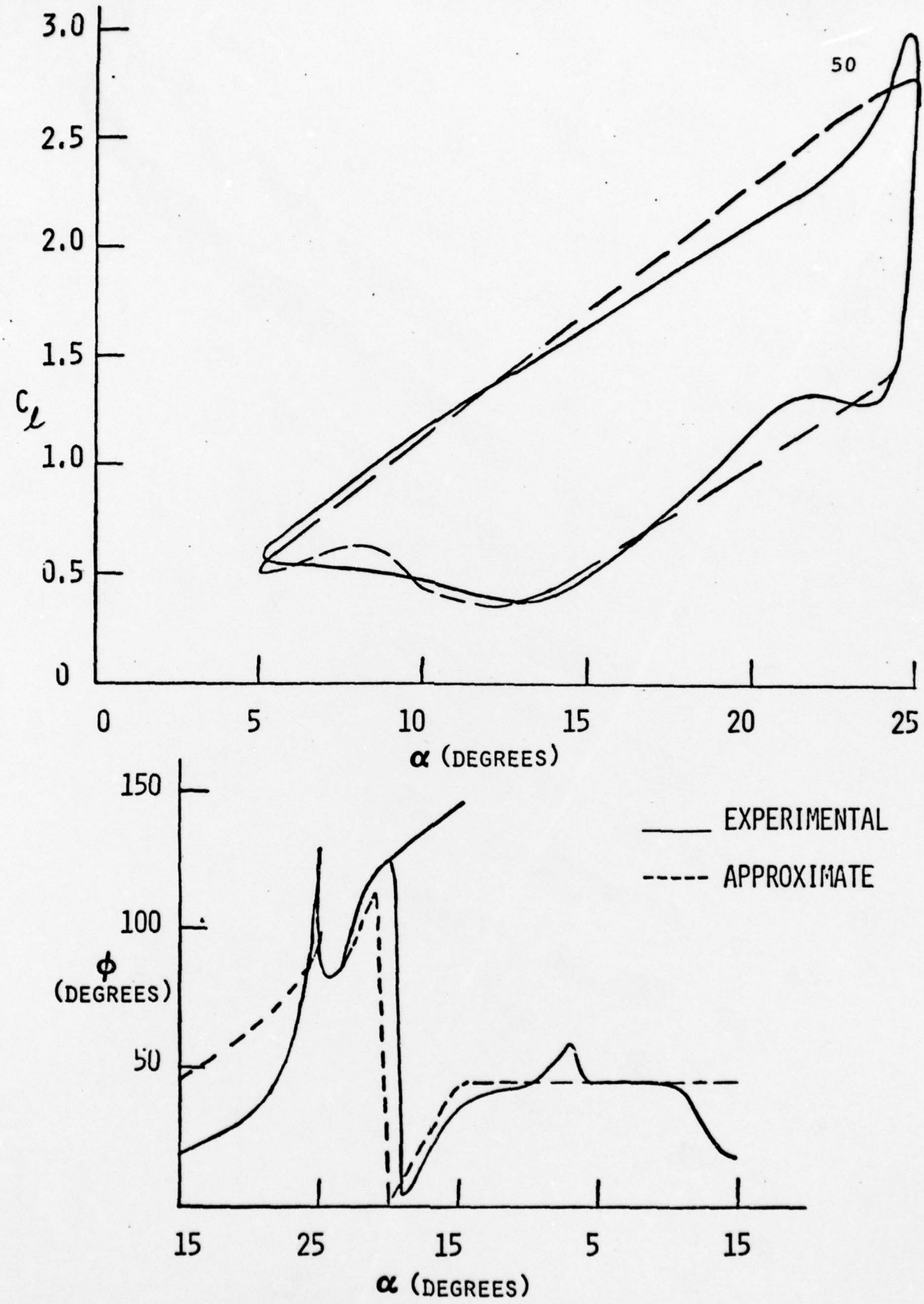

Figure 15. The Phase Lag (ϕ) Distribution over a Complete Cycle to Correlate with Experiment.